DOE/ER/13336-2

CSDP: The Seismology of Continental Thermal Regimes

Final Report

For Period April 1, 1986 - April 1, 1987

Keiiti Aki
Department of Geological Sciences
University of Southern California
Los Angeles, CA 90089-0740

July, 1987

Prepared for

The U.S. Department of Energy
Under Contract No. DE-FG03-85ER13336

DISCLAIMER

DOE/ER/13336--2

DE87 014100

TABLE OF CONTENTS

INTRODUCTION

This is the final report for the project titled "CSDP: Seismology of Continental Thermal Regime". Under the current grant, we have made considerable progress in the study of both wave propagation in complex structures and source mechanism of geothermal seismic events. As described in detail in the next section, we have accomplished the following work in the past one year period.

(1) Interpretation of long-period events observed at Mt. St. Helens and at the Fenton Hill hot dry rock experimental site in terms of seismic radiation from a fluid-filled crack.

(2) Interpretation of teleseismic data collected in and near the Valles caldera in terms of a model with irregular topography, caldera fill, and magma chamber.

(3) Interpretation of VSP (Vertical Seismic Profiling) data from the Oroville fault zone by ray tracing and polarization calculation for P, SV and SH waves in heterogeneous and anisotropic media containing aligned fluid-filled and/or dry cracks.

(4) Development of a new powerful method for calculating seismic motions in media with irregular topography and interfaces by the superposition of Gaussian Beams.

List of Publications in Refereed Journals and Ph.D. Theses Supported by Previous Contract

(DE-AC02-76-ER-02534 and DE-FG03-85-ER-13336)

1. Chouet, B., Source, scattering and attenuation effects on high frequency seismic waves, Ph.D. thesis, Massachusetts Institute of Technology, 183 pp., 1976.
2. Aki, K., M. Fehler, and S. Das, Source mechanism of volcanic tremors: Fluid driven crack models and their application to the 1963 Kilauea eruption, J. Volcan. Geotherm. Res., 2, 259-287, 1977.
3. Aki, K., B. Chouet, M. Fehler, G. Zandt, R. Koyanagi, J. Colp, and R. G. Hay, Seismic properties of a shallow magma reservoir in Kilauea Iki by active and passive experiments, J. Geophys. Res., 83, 2273-2282, 1978.
4. Chouet, B., K. Aki, and M. Tsujiura, Regional variation of the scaling law of earthquake source spectra, Bull. Seis. Soc. Am., 68, 49-79, 1978.
5. Fehler, M., and K. Aki, Numerical study of diffraction of plane elastic waves by a finite crack with application to location of a magma lens, Bull. Seis. Soc. Am., 68, 573-598, 1978.
6. Scheimer, J. F., Experimental study of seismic scattering by a penny-shaped crack, Ph.D. thesis, Dept. of Earth and Planetary Sciences, M.I.T., 1978.
7. Chouet, B., Temporal variation in attenuation of earthquake coda near Stone Canyon, California, Geophys. Res. Letters, 6, 143-146, 1979.
8. Chouet, B., Sources of seismic events in the cooling lava lakes of Kilauea Iki, Hawaii, J. Geophys. Res., 84, 2315-2330, 1979.
9. Fehler, M., Seismological investigation of the mechanical properties of a hot dry rock geothermal system, Ph.D. thesis, Dept. of Earth and Planetary Sciences, M.I.T., 1979.

10. Aki, K., Attenuation of shear-waves in the lithosphere for frequencies from 0.05 to 25 Hz, Phys. Earth Planet. Int., 21, 50-60, 1980.

11. Bouchon, M., Calculation of complete seismograms for an explosive source in a layered medium, Geophysics, 45, 197-203, 1980.

12. Aki, K., Source and scattering effects on the spectra of small local earthquakes, Bull. Seis. Soc. Am., 71, 1687-1700, 1981.

13. Aki, K., and R. Koyanagi, Deep volcanic tremor and magma ascent mechanism under Kilauea, Hawaii, J. Geophys. Res., 86, 7095-7109, 1981.

14. Aki, K., 3-D inhomogeneities in the upper mantle, Tectonophysics, 75, 31-40, 1981.

15. Chouet, B., Ground motion in the near field of a fluid-driven crack and its interpretation in the study of shallow volcanic tremor, J. Geophys. Res., 86, 5985-6016, 1981.

16. Chouet, B., and K. Aki, Seismic structure and seismicity of the cooling lava lake of Kilauea Iki, Hawaii, J. Volcanol. Geotherm. Res., 9, 41-56.

17. Fehler, M., Changes in P wave velocity during operation of a hot dry rock geothermal system, J. Geophys. Res., 86, 2925-2928, 1981.

18. Zandt, G., Seismic images of the deep structure of the San Andreas fault system, central coast ranges, California, J. Geophys. Res., 86, 5039-5052, 1981.

19. Aki, K., Three-dimensional seismic inhomogeneities in the lithosphere and asthenosphere: Evidence for decoupling in the lithosphere and flow in the asthenosphre, Rev. Geophys. Space Physics, 20, 161-170, 1982.

20. Aki, K., M. Fehler, R. L. Aamodt, J. N. Albright, R. M. Potter, C. M. Pearson, and J. W. Tester, Interpretation of seismic data from hydraulic fracturing experiments at the Fenton Hill, New Mexico, hot dry rock geothermal site, J. Geophys. Res., 87, 936-944, 1982.

21. Fehler, M., and B. Chouet, Operation of a digital seismic network on Mount St. Helens volcano and observations of long period seismic events that originate under the volcano, Geophys. Res. Letters, 9, 1017-1020, 1982.

22. Fehler, M., Interaction of seismic waves with a viscous liquid layer, Bull. Seis. Soc. Am., 72, 55-72, 1982.

23. Fehler, M., Using dual-well seismic measurement to infer the mechanical properties of a hot dry rock geothermal system, J. Geophys. Res., 87, 5485-5494, 1982.

24. Chouet, B., Free surface displacements in the near field of a tensile crack expanding in three dimensions, J. Geophys. Res., 87, 3868-3872, 1982.

25. Wu, R. S., Attenuation of short period seismic waves due to scattering, Geophys. Res. Letters, 9, 9-12, 1982.

26. Wu, R. S., Mean field attenuation and amplitude attenuation due to wave scattering, Wave Motion, 4, 305-316, 1982.

27. Chouet, B., Ground motion near an expanding pre-existing crack, J. Volcanol. Geotherm. Res., 19, 367-379, 1983.

28. Aki, K., Evidence for magma intrusion during the Mammoth Lakes earthquakes of May, 1980 and implications of the absence of volcanic (harmonic) tremor, J. Geophys. Res., 89, 7689-7696, 1984.

29. Chouet, B., Excitation of a buried magmatic pipe: a seismic source model for volcanic tremor, J. Geophys. Res., 90, 1881-1893, 1985.

30. Chouet, B., R. Koyanagi and K. Aki, The origin of volcanic tremors, to appear in the U.S.G.S. Professional Paper on Hawaiian Volcanism.

31. Wu, R. and K. Aki, The fractal nature of the inhomogenities in the lithosphere evidenced from seismic scattering, PAGEOPH 123, 805-818, 1985.

32. Lee, W. H. K., K. Aki, B. Chouet, P. Johnson, S. Marks, J. T. Newberry, A. S. Ryall, S. W. Stewart and D. M. Tottingham, A preliminary study of coda Q in California and Nevada, Bull. Seis. Soc. Am., 76, 1143-1150, 1986.

33. Ferrazzini, V. and K. Aki, Slow waves trapped in a fluid-filled infinite crack; Implication for volcanic tremor, in press, J. Geophys. Res., 1987.

34. Ferrazzini, V., K. Aki, B. Chouet, M. Fehler, Very slow waves trapped in a fluid layer with application to the long-period events. Hawaii symposium on How Volcanoes Work, Abstract Volume, Jan. 1987.

Summary Report for the Past Year

(1) Interpretation of long-period events observed at Mt. St. Helens and at the Fenton Hill hot dry rock experimental site in terms of seismic radiation from fluid-filled crack.

Since Fehler (1983) found that volcanic tremor and so called "long-period events" observed at Mt. St. Helens share the same peaked spectrum, the former has come to be regarded as a sequence of randomly occurring long-period events. Recently, Bame and Fehler (1986) showed that the first events which occur during hydraulic fracturing in virgin rock at the Fenton Hill hot dry rock site are long-period events. Fig. 1 compares the long-period events from Mt. St. Helens and Fenton Hill. The similarity in both wave form and spectrum is striking although the time scale differs two orders of magnitude between the two. This similarity naturally suggests that the long-period event and tremor at Mt. St. Helens may also be due to hydraulic fracturing by excess magma pressure (Nakamura, 1977; Aki et al., 1977).

Figure 2 shows observed waveform of several long-period events at Fenton Hill and the corresponding spectra. The diversity of waveform is considerable; all these events have been recorded at the same station within one hour of the start of pressurization. We believe, however, that they are all generated by the same fluid-filled crack because the two lowest frequency peaks are identical for all events. The one at the bottom of Fig. 2 is probably a tremor composed of several long period events.

In order to simulate these events, we used the computer program written by Chouet (1986) who solved the coupled equation of motion for fluid and solid by a finite difference method. As shown on the right hand side of Fig. 3, a fluid-filled crack of rectangular shape with length L and width W is embedded in an isotropic homogeneous unbounded elastic medium. Seismic radiation is excited by the sudden failure of a barrier of area WS as indicated in the same

figure. The failure of the barrier is simulated by applying a step in normal stress over the area ΔS given a short rise time. The fluid flows into the cavity newly created by the opening of the barrier, vibration is set up in the fluid and seismic waves are radiated.

The contour map at the left-hand side of Fig. 3 shows the spectral amplitude of far-field P and S waves as a function of frequency ω and wave number k. The far-field spectrum in the direction θ can be obtained as a cross-section along a straight line passing through the origin ($k=o$, $\omega=o$), with a slope determined by θ. For example, the two lines indicated as "P-radiation" corresponds to $\theta=0$ and $\theta=180°$. The contour map is used for a quick comparison of model prediction and observation. The P-waves farfield displacement and spectra corresponding to three different cases of barrier locations are shown in Fig. 4 for $\theta=30°$. We find that the general appearance of predicted records is quite similar to the observed.

Depending on the location of barrier, excited modes are different. If the barrier is located at a node of a given mode, this mode will not be excited. For example, when the barrier is at the center of the crack, the fundamental mode with wavelength $\lambda=L$ disappears. The character of wave-form changes quite drastically depending on the barrier location. The length of barrier also affects the wave form considerably as shown in Figs. 5 and 6. When the barrier lies along the whole width of the crack (top case), only longitudinal modes are excited, and the amplitudes of spectrum peaks decay regularly with frequency. On the other hand, as the barrier length is shortened, both longitudinal and transverse modes are exited and interact to give rise to strong peaks at intermediate frequencies. This feature can be seen in observed cases as shown in Fig. 2. The case 3 shows a strong peak in the middle of the spectrum while the case 4 shows a regular decay with

increasing frequency.

Thus, we can not only reproduce the general appearance of observed seismogram, but also explain their variability using a single model of fluid filled crack with different trigger locations and geometry.

The model parameters best constrained by the fit to observation are the length L and the width W of the crack. For the episode shown in Fig. 2, L and W are estimated as 5 and 1.25 meters. The thickness of crack can in principle be determined if we can constrain crack stiffness factor C. Although we need more parameter sensitivity study to gain confidence in the estimation of C, C=100 gives a reasonable agreement with observed features of seismograms, and corresponds to the thickness of 5 mm. We also estimated the magnitude of excess pressure from the absolute amplitude of tremor, and obtained a reasonable value of several tens of bars.

Finally, we would like to demonstrate the ubiquity of long-period events and tremors in the world volcanoes by showing the record of unusual events observed at Oshima one year before the recent eruption in Fig. 7. The record is obtained by Ukawa and Ohtake (written communication) and is compared with the Fenton Hill event shown at the bottom of Fig. 2. The similarity is again striking. Since the time scale between the two events differs by a factor of 100, the fluid-filled crack at Oshima should have the size of 500 m x 125 m.

Long-period event

at Mt. St. Helens

on 9- 3-81 (Fehler).

Volcano.

10. *sec.*

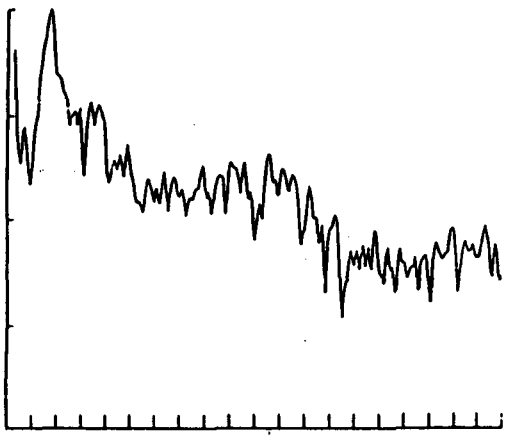

20. *Hz*

inst: 4 ievt: 18 chan: 1 time 0/ 0/ 0 0 0: 0. 0
fft len: 4096 data pts used: 2400 msec skip: 4000
max at freq: 1.8 max value: 0.18E-03
linear freq., min freq: 1.0 max freq: 20.000 tick space: 1
log amplitude plotted, max value is at top, tick marks every decade
bcr5.fft

Long-period event

at Fenton Hill (New Mexico)

on 11- 8-82 (Fehler).

Hydrofracture experiment.

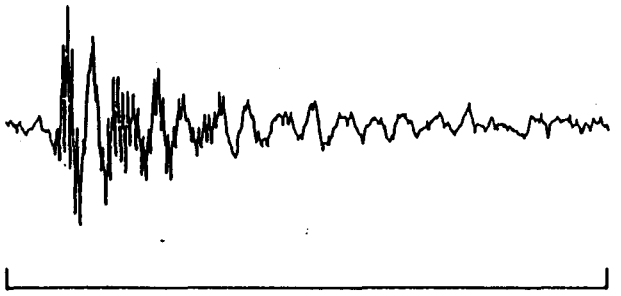

0.15 *sec.*

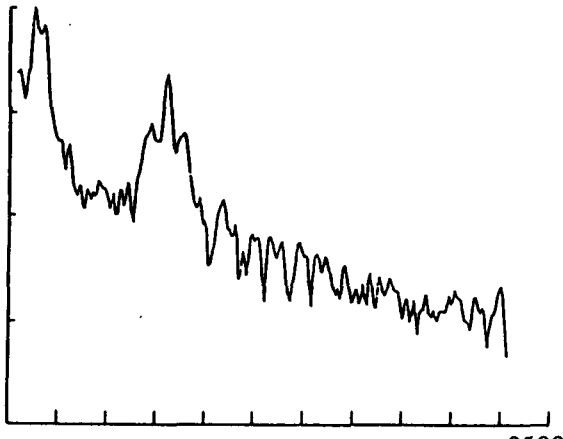

2500. *Hz*

inst: 1 ievt: 11 chan: 1 max at freq: 127.0 max value: 0.66E-09
fft len: 512 data pts used: 500 msec skip: 24
linear freq., min freq: 1.0 max freq: 2500.0 tick space: 249
log amplitude plotted, max value is at top, tick marks every decade

Fig. 1

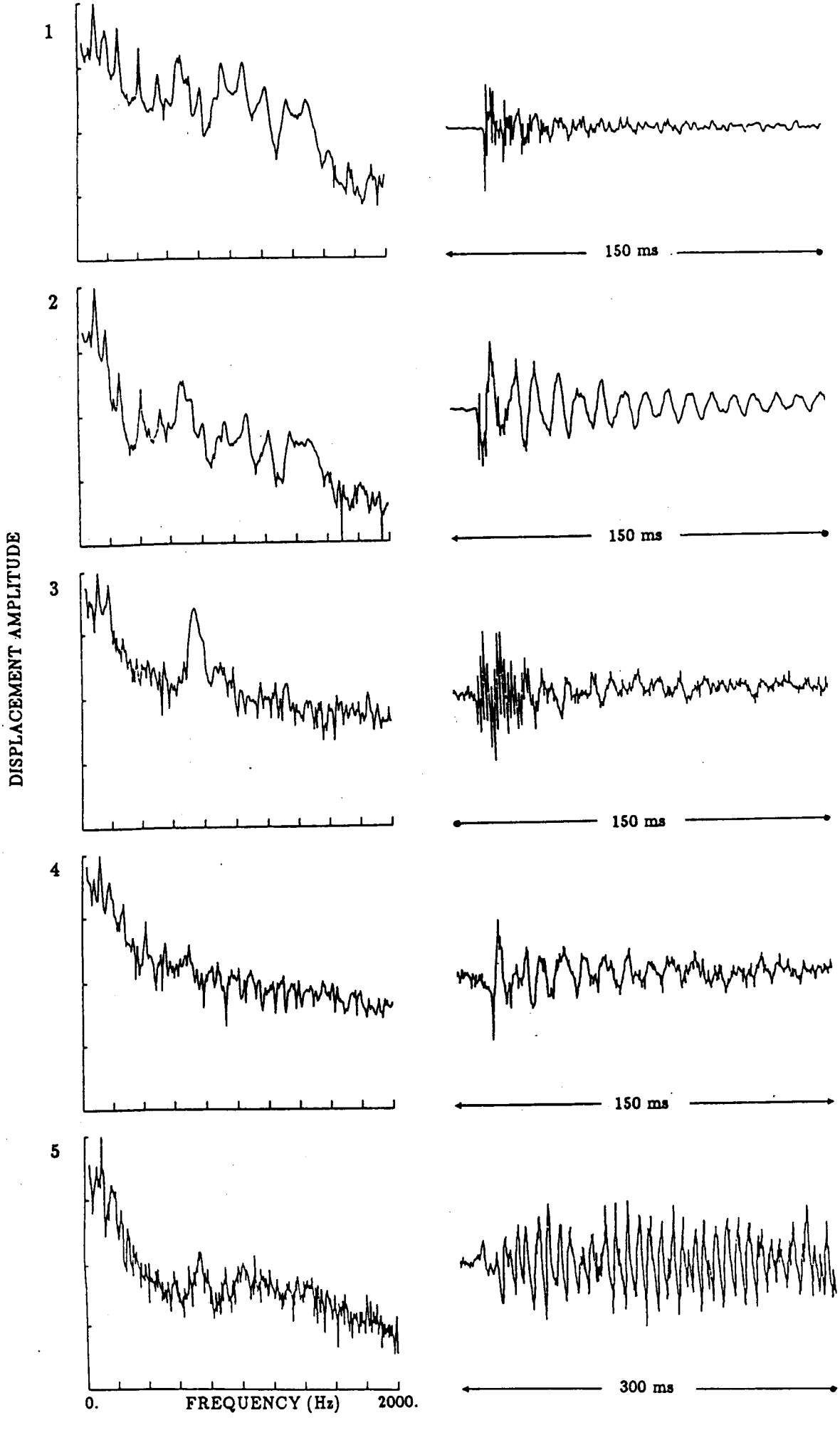
1
2
3
4
5
DISPLACEMENT AMPLITUDE
150 ms
150 ms
150 ms
150 ms
300 ms
0.
FREQUENCY (Hz)
2000.

Fig. 2

$C = 100$

$\phi = 30^o$

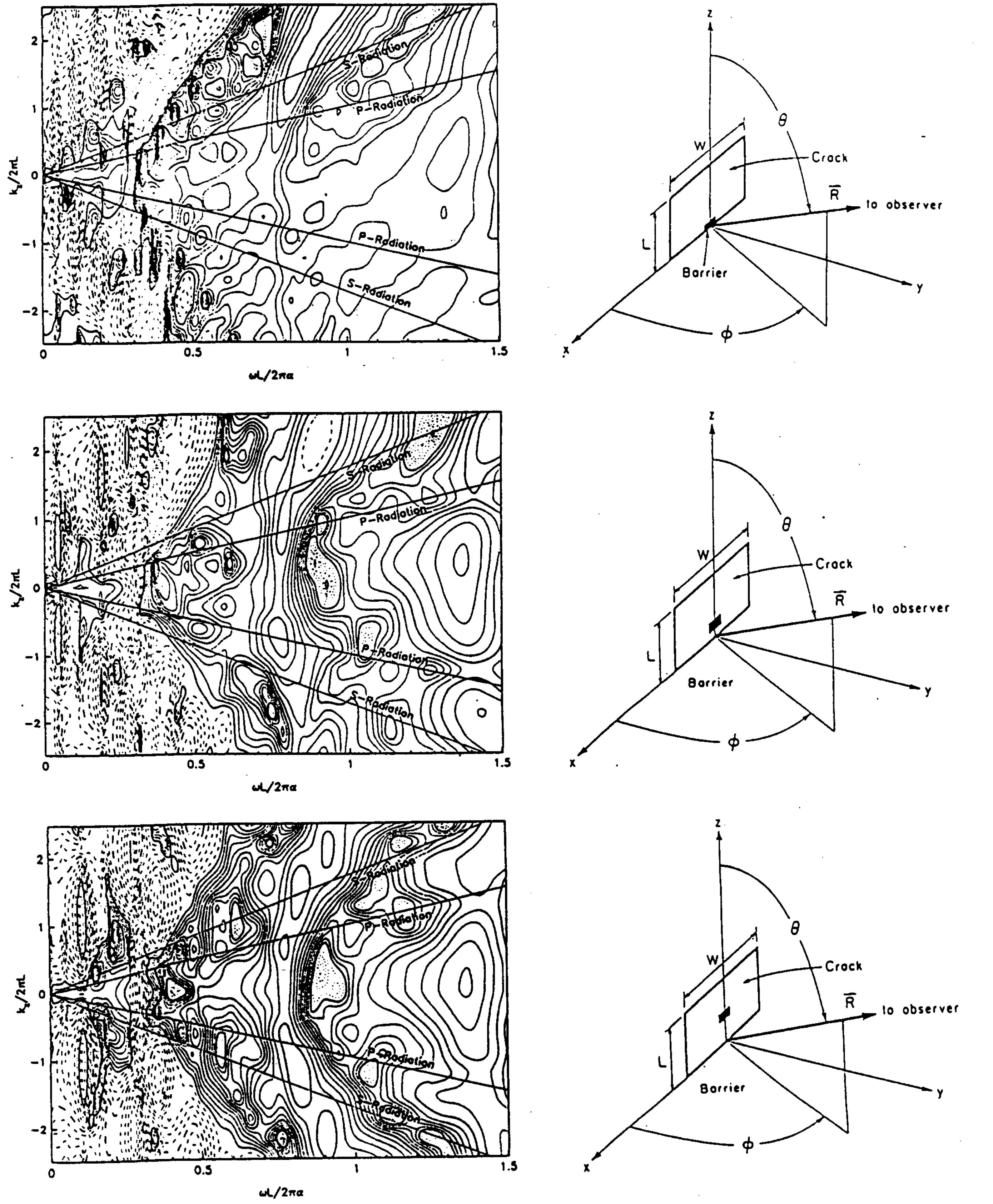

Fig. 3

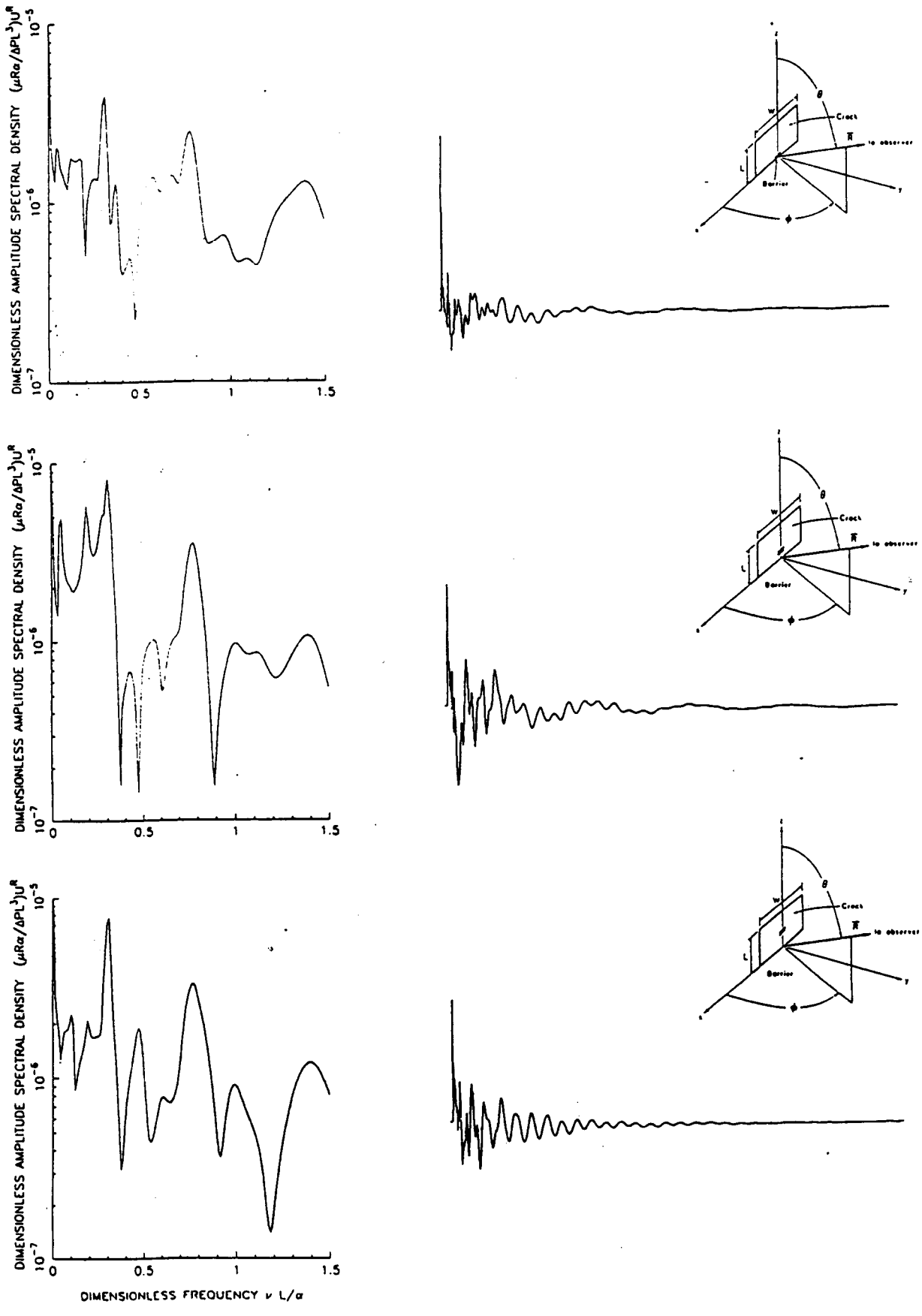
DIMENSIONLESS AMPLITUDE SPECTRAL DENSITY $(\mu Ra/\Delta PL^3)U^R$
10^{-5}
10^{-6}
10^{-7}
0
0.5
1
1.5
DIMENSIONLESS FREQUENCY ν L/a
Crack
Barrier
to observer

Fig. 4

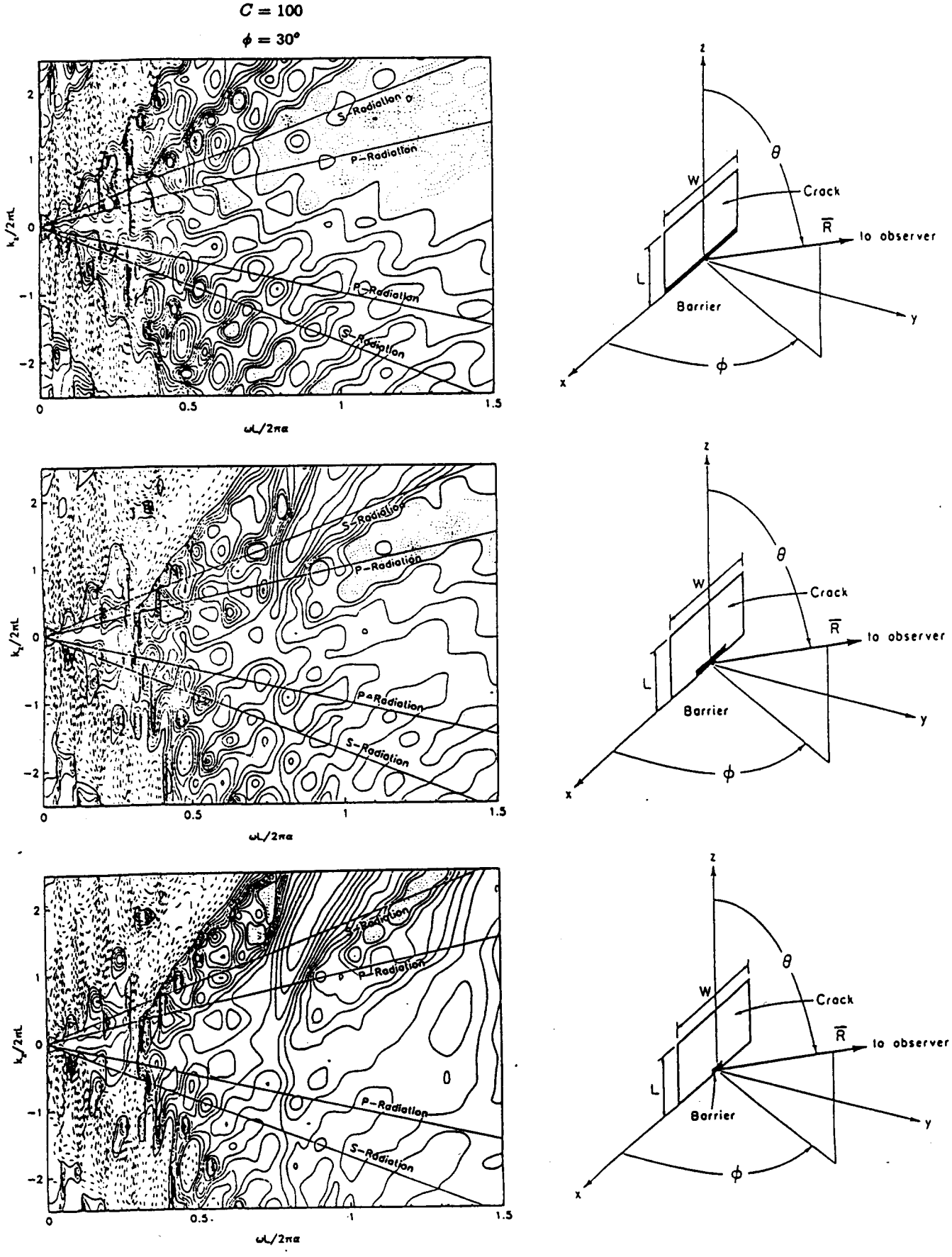
C = 100
φ = 30°
S-Radiation
P-Radiation
P-Radiation
S-Radiation
k_z/2πL
ωL/2πα
0
0.5
1
1.5
2
1
0
-1
-2
z
θ
W
Crack
R̄
to observer
L
Barrier
y
x
φ

Fig. 5

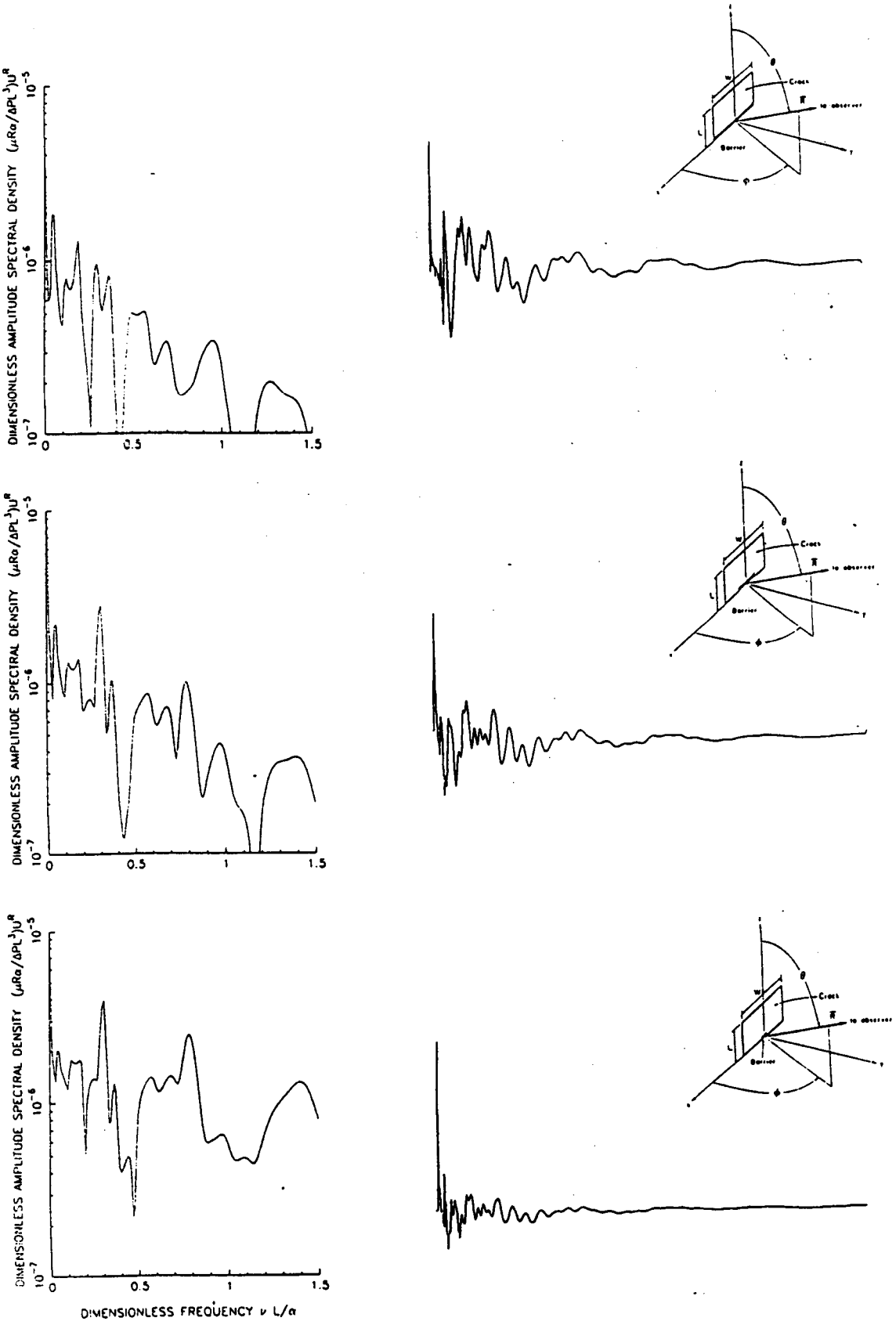
DIMENSIONLESS AMPLITUDE SPECTRAL DENSITY (μRa/ΔPL³)U^R
10⁻⁵
10⁻⁶
10⁻⁷
0
0.5
1
1.5
DIMENSIONLESS FREQUENCY ν L/a
Barrier
to observer

Fig. 6

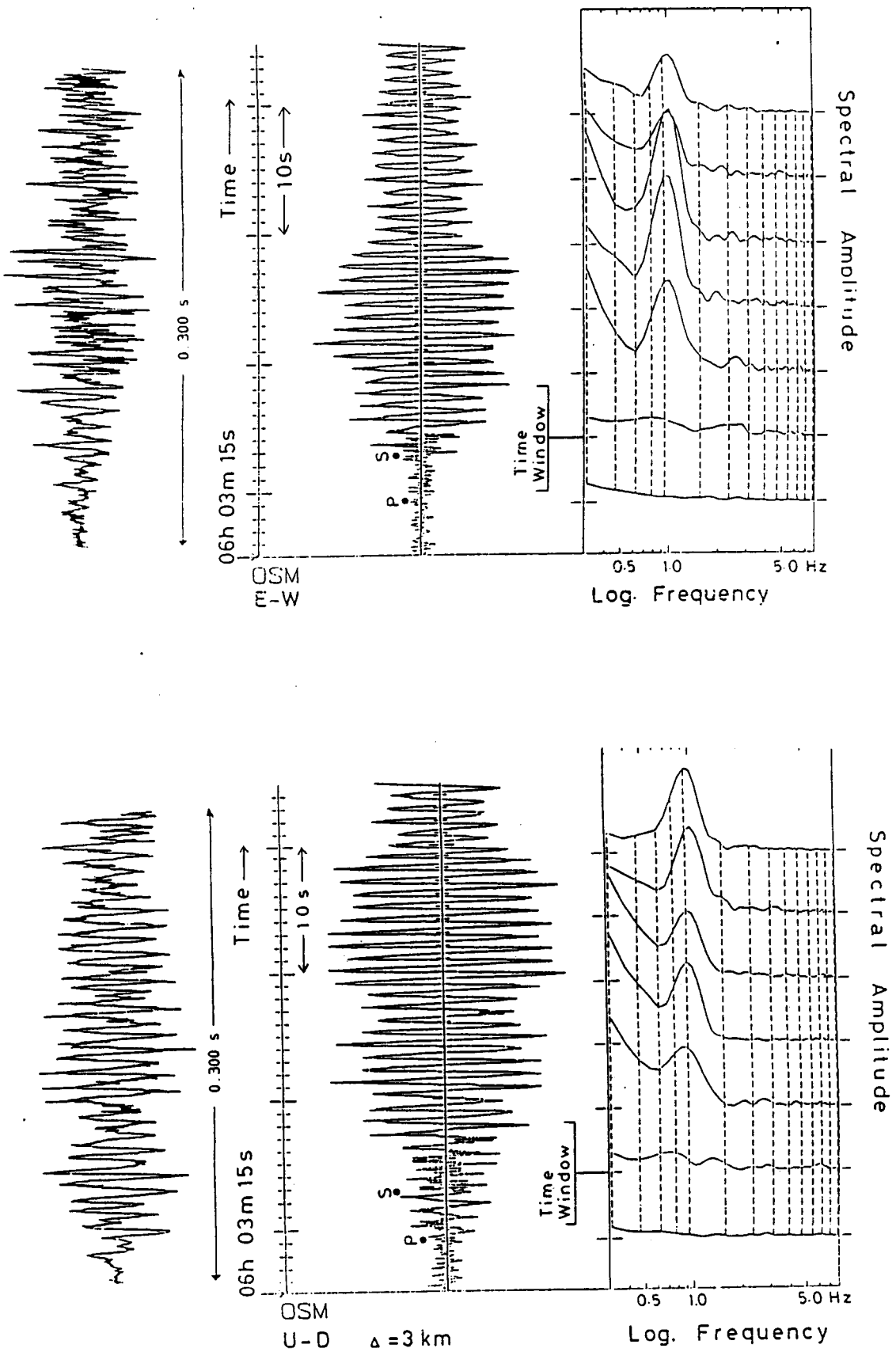
0.300 s
Time
10s
06h 03m 15s
OSM
E-W
S
P
Time Window
Spectral Amplitude
0.5
1.0
5.0 Hz
Log. Frequency
0.300 s
Time
10 s
06h 03m 15s
OSM
U-D
Δ=3 km
S
P
Time Window
Spectral Amplitude
0.5
1.0
5.0 Hz
Log. Frequency

Fig. 7

(2) Interpretation of teleseismic data collected in and near the Valles caldera in terms of a model with irregular topography, caldera fill and magma chamber.

Figure 1 shows a map view of the site occupied by six 3-component digital event recorders in the Jemez Mts. during the field experiment in the summer and fall of 1986. The sites in the Valles caldera at RDT, JAR and PDA were moved to FLK, BRY and WAC for the second half of the experiment. The three eastern sites PIP, GRE and GCA were maintained throughout the entire experiment. The linearity and azimuth of the array were chosen with the aim of recording normally incident teleseimic events from the Tonga Trench for comparison with the synthetic results computed by the method of Aki and Larner (1970) for an appropriate caldera model. By adjusting the model until a good fit is obtained we intend to obtain an accurate profile of P and S-wave velocity for the caldera and underlying structure including the presumed magma chamber.

Figure 2 shows the free surface topography model used in the synthetic calculations. The locations of the nine field sites in Figure 1 are also indicated. The Aki-Larner method produces estimates of the displacement field, in the frequency domain, at x-coordinates along the free surface of the model and comparisons with observed data are made at the positions corresponding to the field sites. Figure 3 shows one possible choice for the full 3-layered model geometry. The model is defined from x=o to x=256 km with the interface irregularities confined to a 40 km interval centered at x=128 km. We have been testing this and other geometries with various degrees of interface contrasts and incident wave frequencies to attempt the fit with real data. We have used what information exists about possible interface shapes and locations and about possible velocities and densities for the media in each layer. The surficial layer is low velocity caldera fill and its

thickness and velocities are fairly well known. We model the magma chamber as a low velocity intrusion into an otherwise uniform granite basement, assigning the same medium parameters to both layer 2 and the halfspace. Since little conclusive evidence exists concerning the size, shape and velocities in the magma body we believe that these three aspects of the model are more freely adjustable than those defining the granite basement, caldera fill or surface topography. We have set about isolating those features of the free surface displacement profile which can be attributed mainly to interaction with the magmas by examining several simpler models.

Using the model in Figure 3 as a start we generated the displacement profiles for two different frequencies of plane P-waves normally incident in the halfspace. Figure 4 shows the results for f=0.5 and 1.0 Hz for the vertical and horizontal components of motion. All plots of this kind are shown normalized by the vertical component solution for the corresponding problem in which all interface irregularities are removed (flat layer problem). The plot amplitudes then represent amplification or attenuation relative to the flat layer solution. The plots in Figure 4 are complicated by dominant effects of the surficial layer and surface topography and it is difficult to assign any features to the magma chamber. Figure 5 shows results for the same model with the surface topography removed. Figure 6 shows the 0.5 Hz plot of Figure 5 along with the results obtained with the surficial layer and magma chamber removed in turn. Here we can see that the surficial layer produces the peak amplitude in the vertical component but the magma chamber is primarily responsible for the peaks in the horizontal component.

Also the vertical component shows zones of mild attenuation at about x=112 and 144 km and a significant drawdown of the peak amplitude, both of which are clearly caused by the magma chamber. These effects increase with increasing contrast between the granite and magma and eventually will produce attenuation in the vertical component at x=128 km for f=0.5 Hz. Concurrently the peaks in the horizontal component will grow until vertical and horizontal amplitudes overlap. These numerical experiments help to design future field experiments for crucial observations.

During the 1986 field experiment we recorded a magnitude 6.0 teleseism from the Tonga Trench at sites RDT, JAR, PIP, GRE and GCA. All sites except GRE displayed horizontal motions comparable in amplitude to the vertical component. Since Tonga is far enough away (delta = 88 degrees) to assume nearly vertical incidence for waves arriving below the caldera model we assumed the horizontal motion to be due to scattered waves generated by the caldera sub-structure. The GRE vertical record was used as the reference in the spectral ratios because scattering was the least at GRE. The north-south components were ignored since the synthetic solutions for P-SV scattering problems only give motions parallel to the x-z model plane.

The spectral ratios at 0.2, 0.5 and 1.0 Hz are summarized in the following table.

Table 1. Spectral Ratios

		RDT	JAR	PIP	GRE	GCA
1 Hz	V	0.5	0.3	3.0	1.0	0.5
	---	---	---	---	---	---
	H	2.0	0.3	0.3		0.2
0.5 Hz	V	0.6	0.5	0.5	1.0	0.5
	---	---	---	---	---	---
	H	1.0	0.5	1.0		0.5
0.2 Hz	V	0.4	0.6	1.0	1.0	1.0
	---	---	---	---	---	---
	H	0.2	0.4	0.8		(1.0)

The most interesting result from Table 1 is that the vertical component amplitudes at stations within Caldera (RDT and JAR) are lower than at stations located on the rim or outside. As shown earlier by the numerical experiment, we know that the topography and magma chamber have the effect of reducing vertical component amplitude, but the caldera fill have the effect of increasing it. Our observation appears to support that the former effect is stronger than the latter.

The observed horizontal-component amplitude should further resolve the question. Their spatial pattern at 0.5 and 1 Hz is, however, somewhat erratic, and cannot give conclusive results. On the other hand, the amplitude at 0.2 Hz shows a systematic increase toward the rim consistent with the effect of magma chamber as shown in Fig. 6.

Thus, our preliminary results suggest the presence of magma chamber under the caldera. Further numerical experiments and additional observations would give us more definitive results on the geometry and seismic properties of the mayma chamber.

1986 SITE LOCATIONS

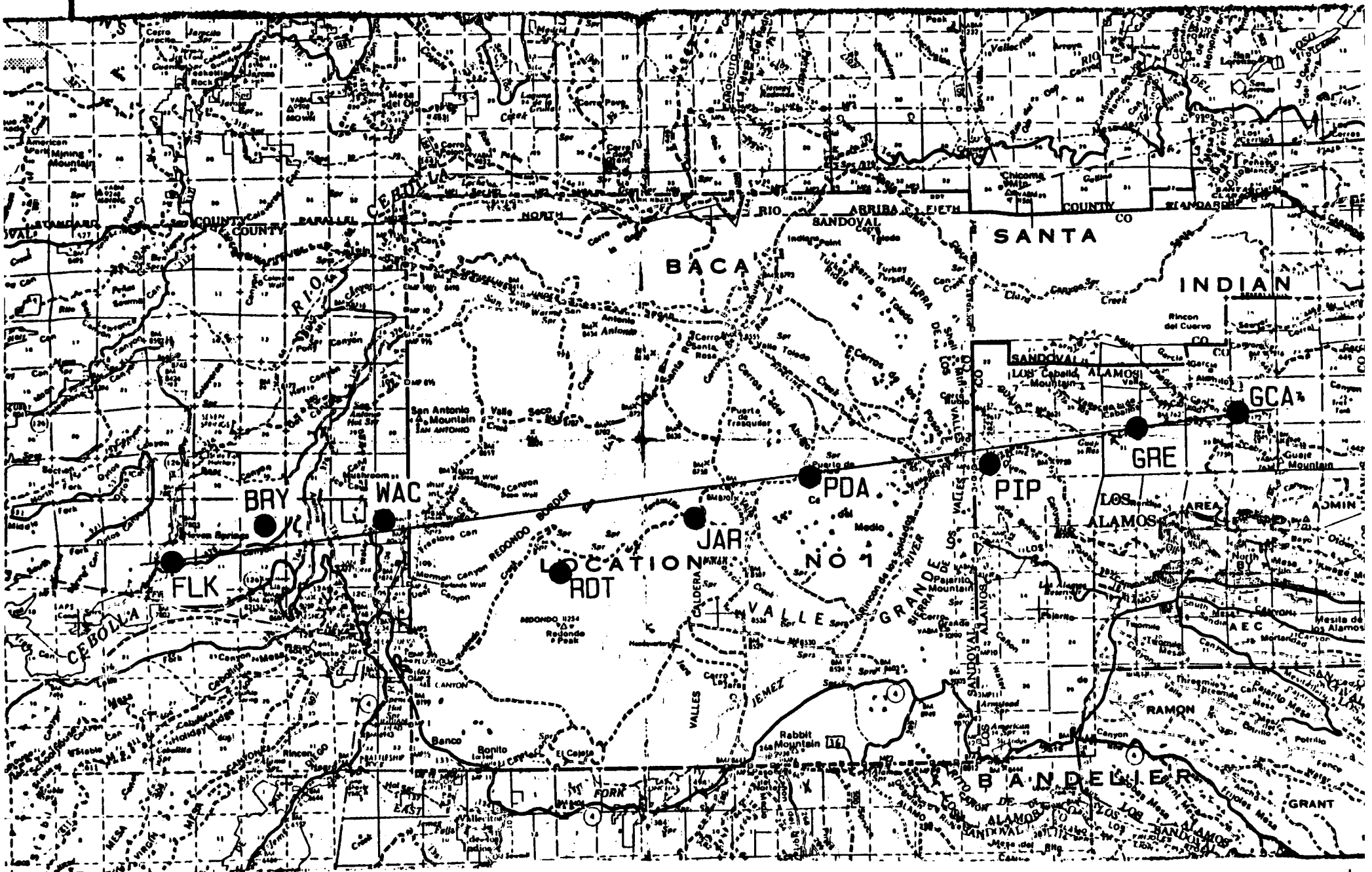

Figure 1.

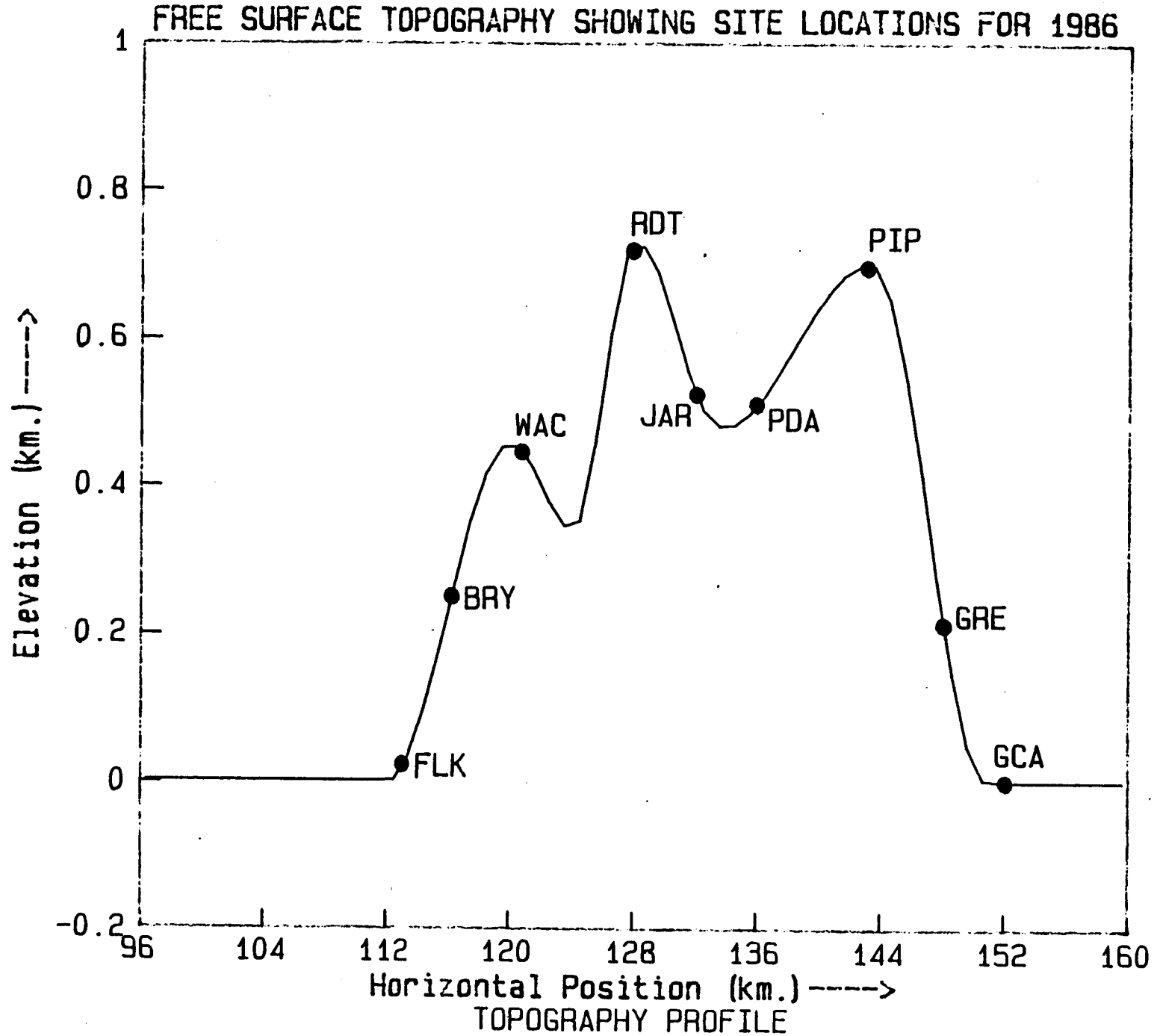
FREE SURFACE TOPOGRAPHY SHOWING SITE LOCATIONS FOR 1986
Elevation (km.)---->
1
0.8
0.6
0.4
0.2
0
-0.2
96
104
112
120
128
136
144
152
160
Horizontal Position (km.)---->
TOPOGRAPHY PROFILE
FLK
BRY
WAC
RDT
JAR
PDA
PIP
GRE
GCA

Figure 2.

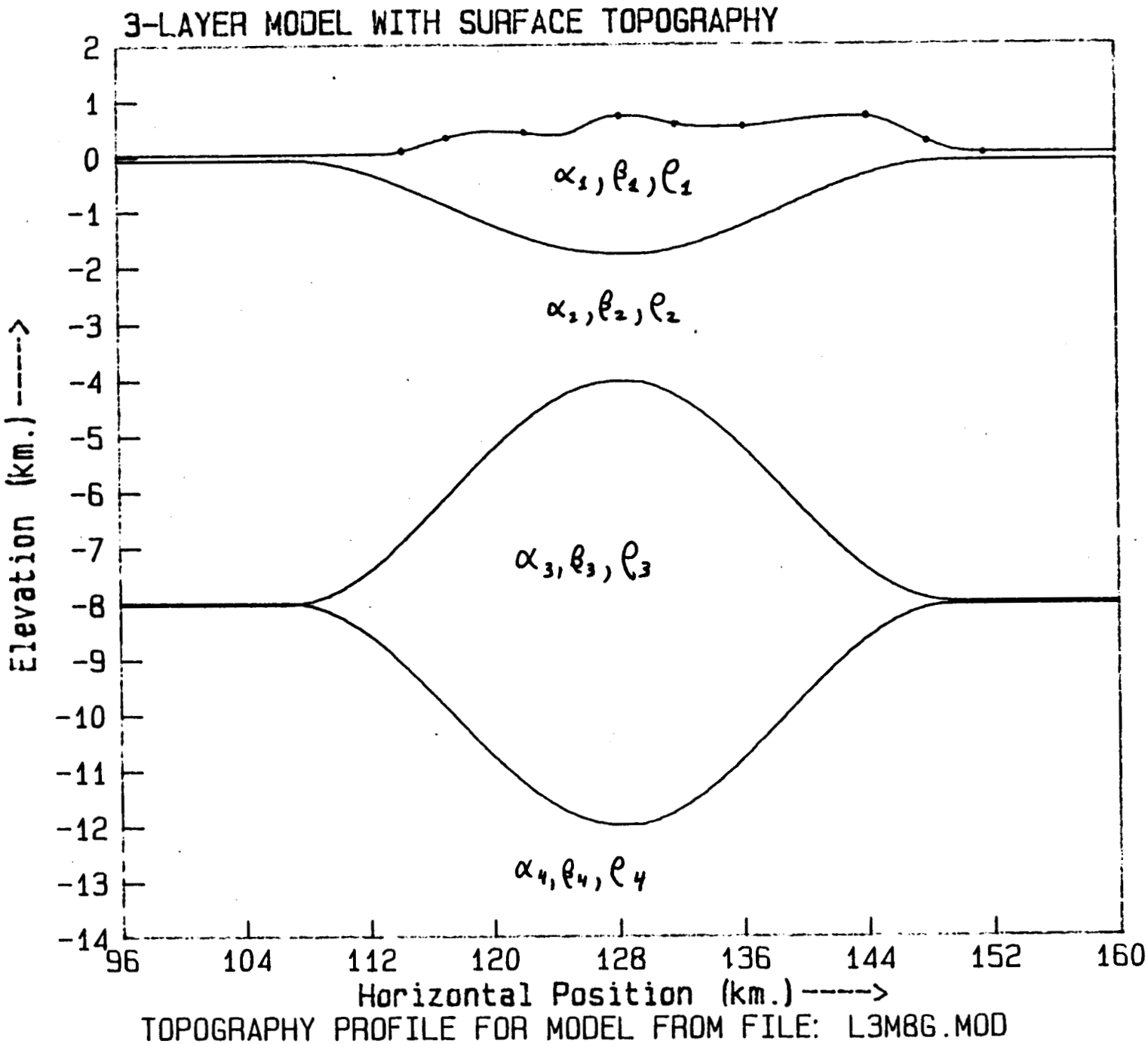
3-LAYER MODEL WITH SURFACE TOPOGRAPHY
Elevation (km.) ----->
2
1
0
-1
-2
-3
-4
-5
-6
-7
-8
-9
-10
-11
-12
-13
-14
$\alpha_1, \beta_1, \rho_1$
$\alpha_2, \beta_2, \rho_2$
$\alpha_3, \beta_3, \rho_3$
$\alpha_4, \beta_4, \rho_4$
96
104
112
120
128
136
144
152
160
Horizontal Position (km.) ----->
TOPOGRAPHY PROFILE FOR MODEL FROM FILE: L3M8G.MOD

Figure 3.

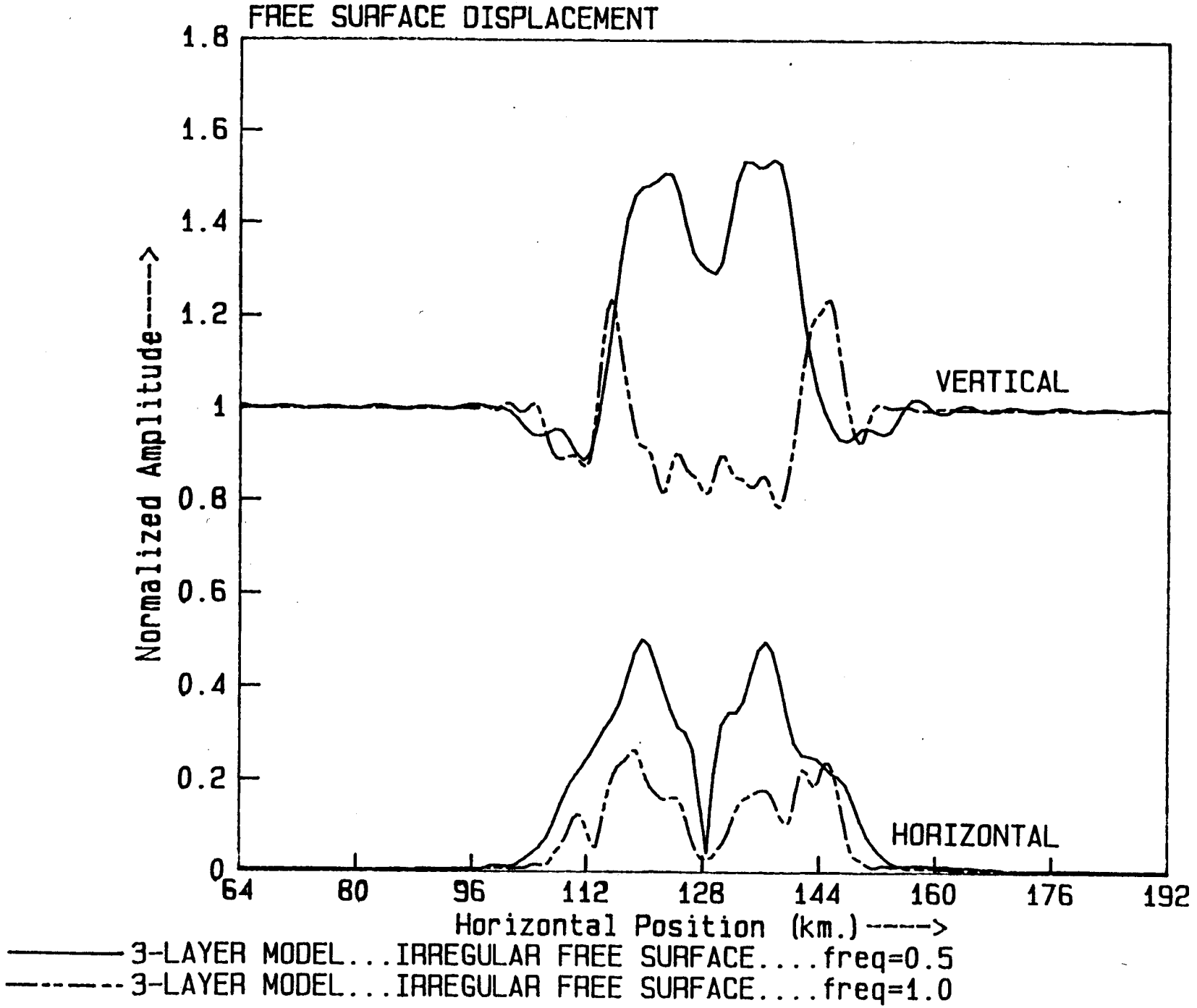
FREE SURFACE DISPLACEMENT
1.8
1.6
1.4
1.2
1
0.8
0.6
0.4
0.2
0
Normalized Amplitude---->
VERTICAL
HORIZONTAL
64
80
96
112
128
144
160
176
192
Horizontal Position (km.)----->
3-LAYER MODEL...IRREGULAR FREE SURFACE....freq=0.5
3-LAYER MODEL...IRREGULAR FREE SURFACE....freq=1.0

Figure 4.

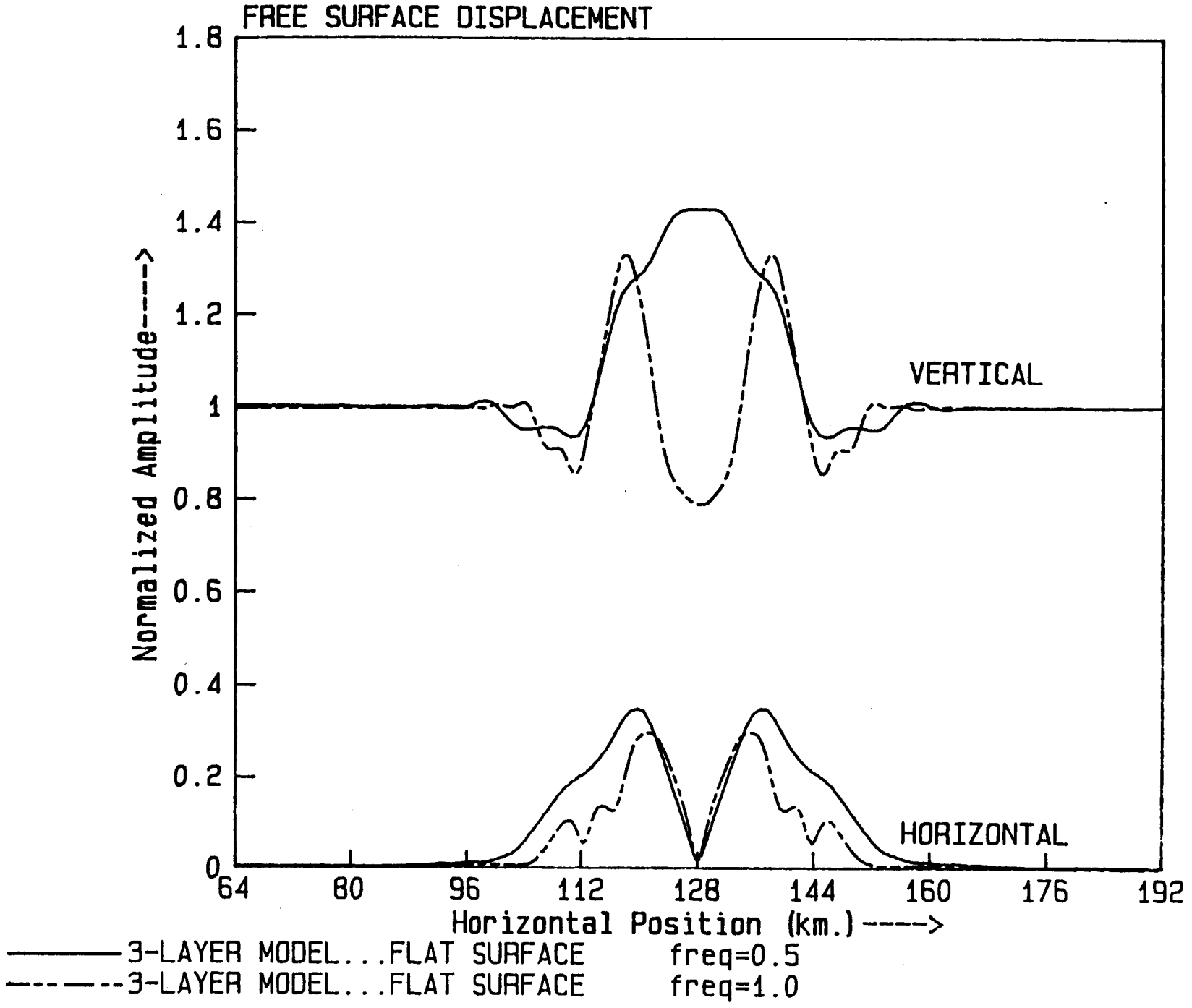
FREE SURFACE DISPLACEMENT
Normalized Amplitude---->
1.8
1.6
1.4
1.2
1
0.8
0.6
0.4
0.2
0
VERTICAL
HORIZONTAL
64
80
96
112
128
144
160
176
192
Horizontal Position (km.)---->
3-LAYER MODEL...FLAT SURFACE freq=0.5
3-LAYER MODEL...FLAT SURFACE freq=1.0

Figure 5.

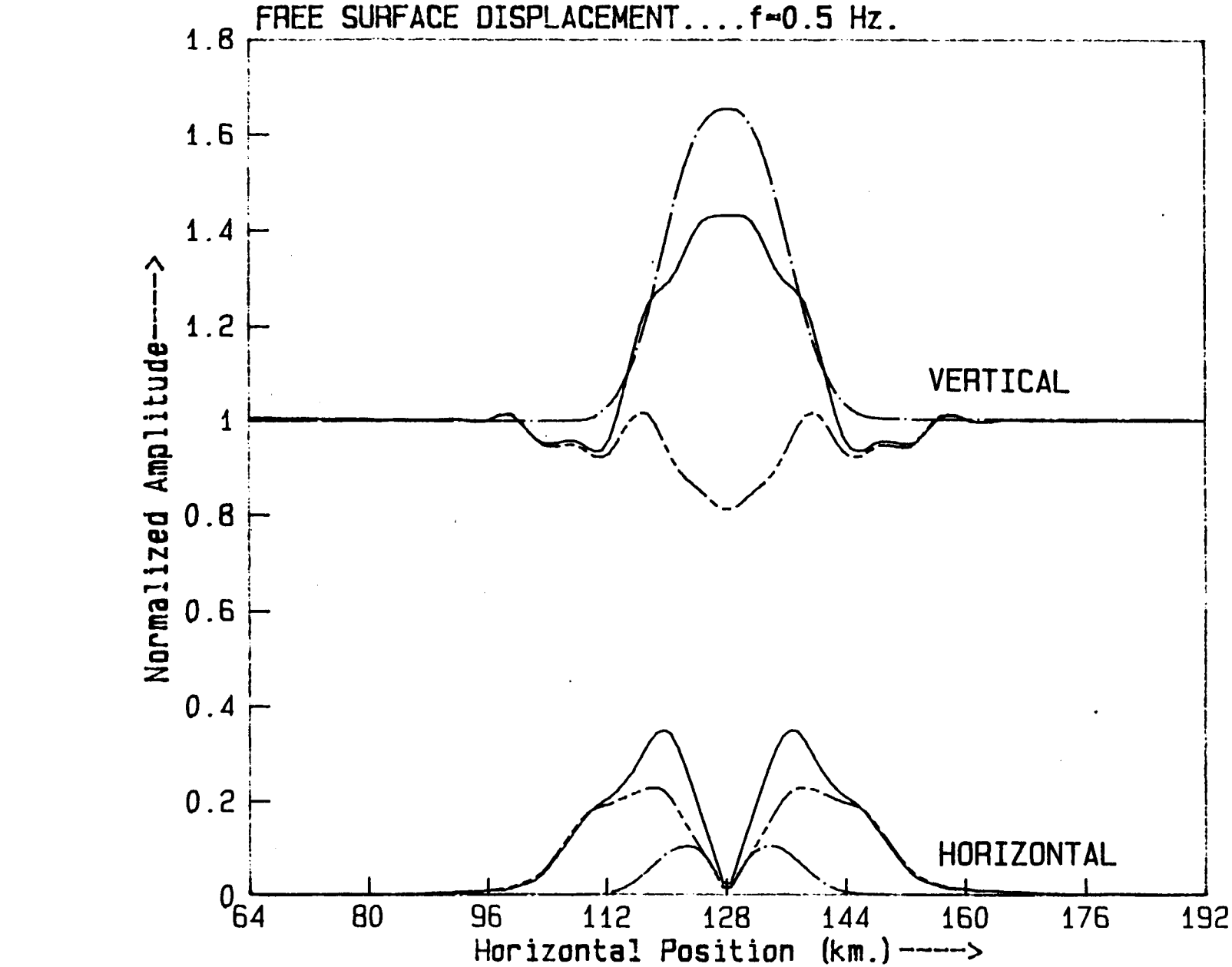
FREE SURFACE DISPLACEMENT....f=0.5 Hz.
Normalized Amplitude---->
1.8
1.6
1.4
1.2
1
0.8
0.6
0.4
0.2
0
VERTICAL
HORIZONTAL
64
80
96
112
128
144
160
176
192
Horizontal Position (km.)----->
FULL 3-LAYER MODEL...FLAT SURFACE
SURFICIAL LAYER REMOVED (MAGMA CHAMBER ONLY)
MAGMA CHAMBER REMOVED (SURFICIAL LAYER ONLY)

Figure 6

(3) Interpretation of VSP data in terms of a heterogeneous anisotropic medium containing aligned cracks.

A multi-offset and multi-depth 3-component VSP (Vertical Seismic Profiling) survey was carried out in a hole in Oroville, California, drilled through a fault zone where an earthquake occurred in 1975. The borehole seismograph may be oriented and pinned securely against the borehole wall. We used a weight-dropping seismic source called "thumper". The seismograph was placed at various depths and the thumper walked away from the top of the hole toward and perpendicular to the surface trace of the fault as schematically shown in Fig. 1.

The observed 3-component records were rotated in such a way that the radial component (P) parallel to the ray path, the horizontal component (SH) perpendicular to ray path and the SV component orthogonal to P and SH are separated on the basis of an initial model of velocity distribution. Some of the observed P, SV, and SH records are shown in Fig. 2. The thumper generated coherent SH waves probably because of the interaction with the near-surface anisotropy with non-vertical axis of symmetry.

We observed a very clear shear-wave splitting: SH waves arrived earlier than SV waves roughly by 0.05 ms per 1 meter of propagation path. Qualitatively, this can be explained by dry or wet cracks aligned parallel to the fault zone. In order to obtain a quantitative result, we modeled the

medium by an elastic body with elastic constants C_{ij}, (i,j=1,2...6), given by

$$C_{ij} = \overset{0}{C}_{ij} + \overset{1}{C}_{ij} \qquad (1)$$

where $\overset{0}{C}_{ij}$ is an isotropic elastic constant, and $\overset{1}{C}_{ij}$ is the anisotropic perturbation due to the presence of aligned cracks.

Following Hudson (1981), we have

$$\overset{1}{C}_{ij} = \frac{-e}{\mu} \begin{bmatrix} \lambda^2 & \lambda^2 & \lambda(\lambda+2\mu) & & & 0 \\ \lambda^2 & \lambda^2 & \lambda(\lambda+2\mu) & U_{33} & & \\ \lambda(\lambda+2\mu) & \lambda(\lambda+2\mu) & (\lambda+2\mu)^2 & & & \\ & & & 2\mu^2 & & 0 \\ 0 & & & & 2\mu^2 & U_{11} \\ & & & 0 & & 0 \end{bmatrix} \qquad (2)$$

here $U_{11} = 16/3\ (\lambda+2\mu)/(3\lambda+4\mu)$ and $U_{33} = 4/3\ (\lambda+2\mu)/(\lambda+\mu)$ and e is the crack density. The crack density is defined by O'Connell and Budiansky (1974) and is equal to $N\langle a^3\rangle$ for circular cracks, where N is the number of cracks in unit volume, and a is the radius of crack. We assumed that the crack density e is a function of distance from the fault plane, and expressed the variation by simple curves specified by a small number of parameters.

We used the ray tracing system described by Cerveny and Psencik (1972) for a two-dimensional anisotropic heterogeneous medium. For a point (x,z) on a ray path and a slowness vector (p,q), the equation for ray tracing, with

travel time, as the independent variable can be written as

$$\frac{dx}{d\tau} = p\,(A_{11} + A_{55} - 2A_{11}A_{55}\,p^2 + A\,q^2) \,/\, D$$

$$\frac{dz}{d\tau} = q\,(A_{33} + A_{55} - 2A_{33}A_{55}\,q^2 + A\,p^2) \,/\, D$$

$$\frac{dp}{d\tau} = -\{\partial A_{11}/\partial X\; p^2\, D_2 + \partial A_{33}/\partial X\; q^2\, D1 + \partial A_{55}/\partial X\; F + 2\partial A_{13}/\partial X\; p^2q^2\,(A_{13} + A_{55})\} \,/\, 2D$$

$$\frac{dq}{d\tau} = -\{\partial A_{11}/\partial_z\; p^2\, D^2 + \partial A_{33}/\partial_z\; q^2\, D1 + A_{55z}\, F + 2\partial A_{13}/\partial z\; p^2q^2\,(A_{13} + A_{55}\} \,/\, 2D$$

for P-SV waves, and

$$\frac{dx}{d\tau} = p\,A_{66}$$

$$\frac{dz}{d\tau} = q\,A_{44}$$

$$\frac{dP}{d\tau} = -1/2\,(\partial A_{66}/\partial x\; p^2 + \partial A_{44}\partial x\; q^2)$$

$$\frac{dq}{d\tau} = -1/2\,(\partial A_{66}/\partial_z\; p^2 + \partial A_{44}/\partial z\; q^2)$$

for SH waves, where

$$D_1 = 1 - A_{11}\, p^2 - A_{55}\, q^2,\ D_2 = 1 - A_{55}\, p^2 - A_{33}\, q^2$$

$$A = A_{13}^2 + 2A_{13}\, A_{55} - A_{11}\, A_{33},\ D = D_1 + D_2$$

$$F = p^2 + q^2 - A_{11}\, p^4 - A_{33}\, q^4 + 2p^2q^2\, A_{13},$$

and $A_{ij} = C_{ij}/\rho$.

There are three vectors associated with the waves in anisotropic medium. The first is the group velocity with components $(dx/d\tau, dz/d\tau)$. The second is the direction of the propagation of wave front, or the slowness vector with components (p,q). The last one is the direction of particle motion, or polarization vector. This is determined by solving the eigen-value and eigen-vector problem for plane harmonic waves in anisotropic media (Aki and Richards, 1980, p. 185).

Using the above equations, we formulated an inverse problem for the travel time P, SV and SH waves. Fig. 3, 4 and 5 shows the fit of observed (dots) and calculated times (curves in the inset) for typical ray paths for the case of P, SV and SH respectively. Final result is shown in Fig. 7, where the crack density is plotted as a function of distance from the fault. We find that

(1) the maximum crack density at the center of fault zone is 7%,

(2) the effective width of the fault zone is about 25 m, and

(3) although the crack density decreases with distance from the fault, the hanging wall contains much more cracks than the foot wall.

The comparison of observed and calculated polarization vector of first P waves also supported the model determined from travel time data as shown in Fig. 6. The model explains well some extraordinary observations such as the reversal of the sign of first motion with the depth of seismograph.

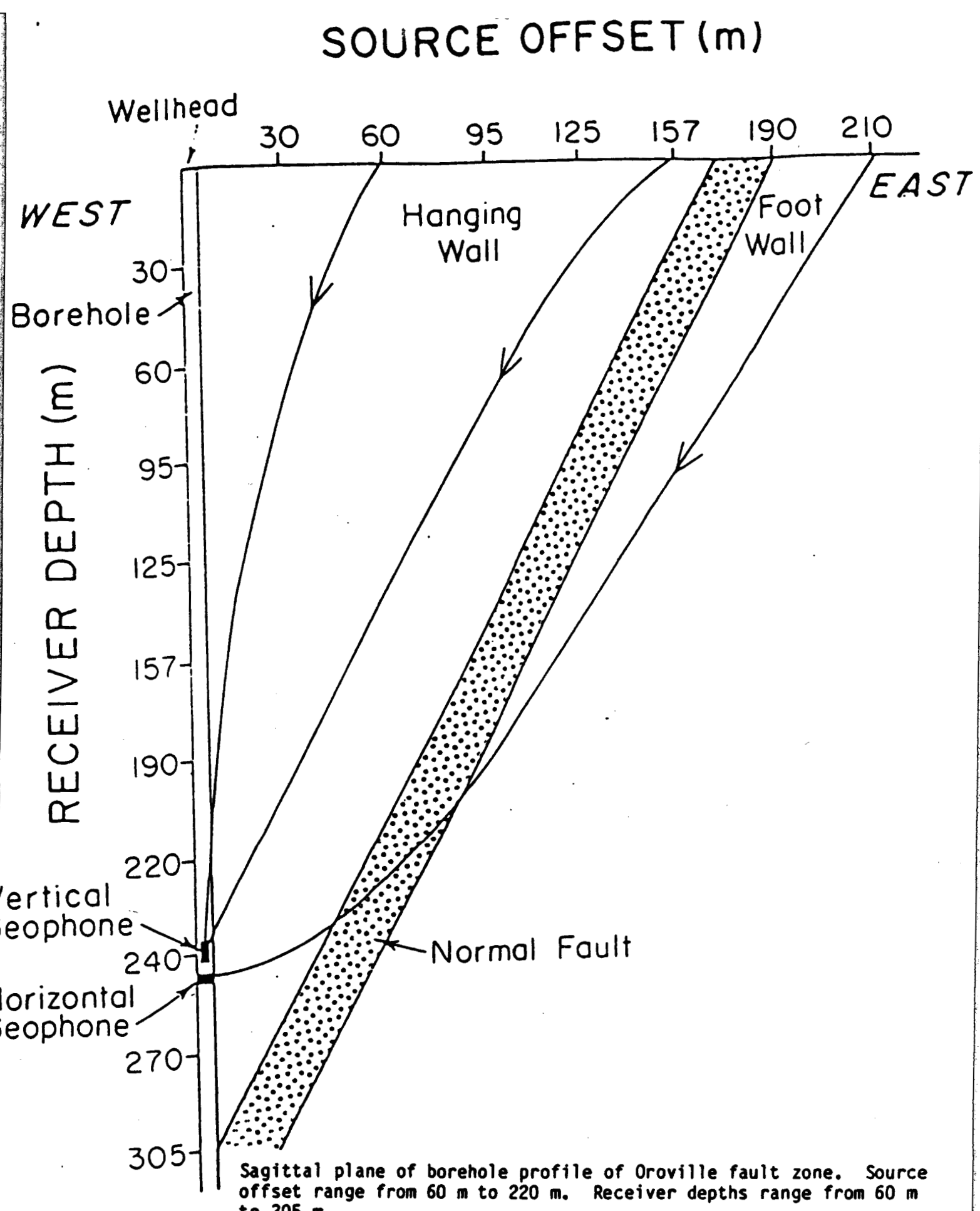

Sagittal plane of borehole profile of Oroville fault zone. Source offset range from 60 m to 220 m. Receiver depths range from 60 m to 305 m.

Fig. 1

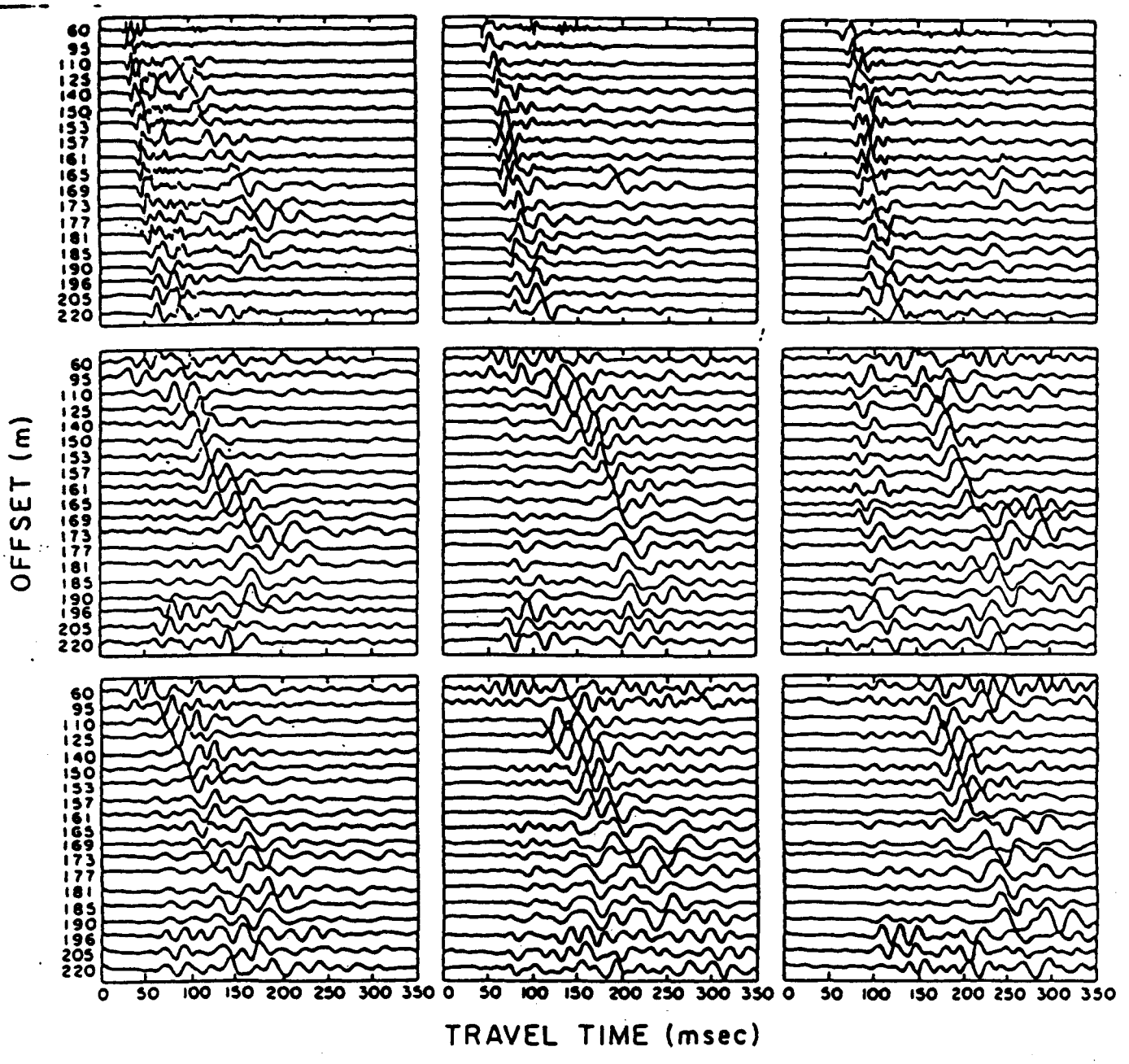

Normalized amplitude seismic grains at three borehole depths for fault range of source offsets. Rows are from top to bottom, P (along ray path), SV (normal to ray path, in sagittal plane), and SH (normal to sagittal plane. Columns are, left to right, depths 90 m, 210 m, and 305 m. Note the transition from hanging wall to footwall denoted by early arrivingd energy at the bottom of each panel. Note also the clear velocity difference between SH and SV energy at lower receiver locations.

Fig. 2

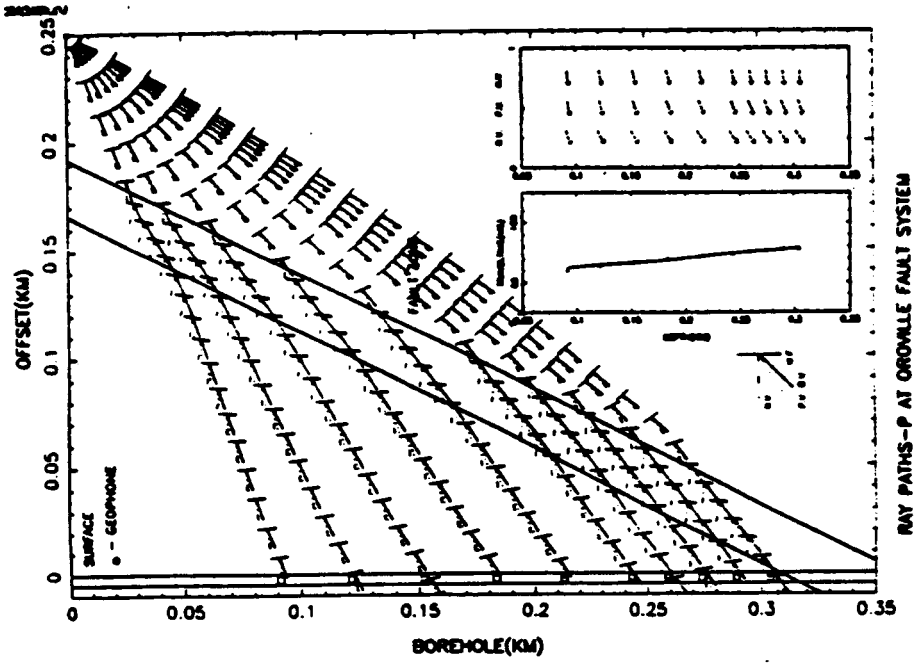
OFFSET(KM)
BOREHOLE(KM)
SURFACE
• - GEOPHONE
RAY PATHS-P AT OROVILLE FAULT SYSTEM

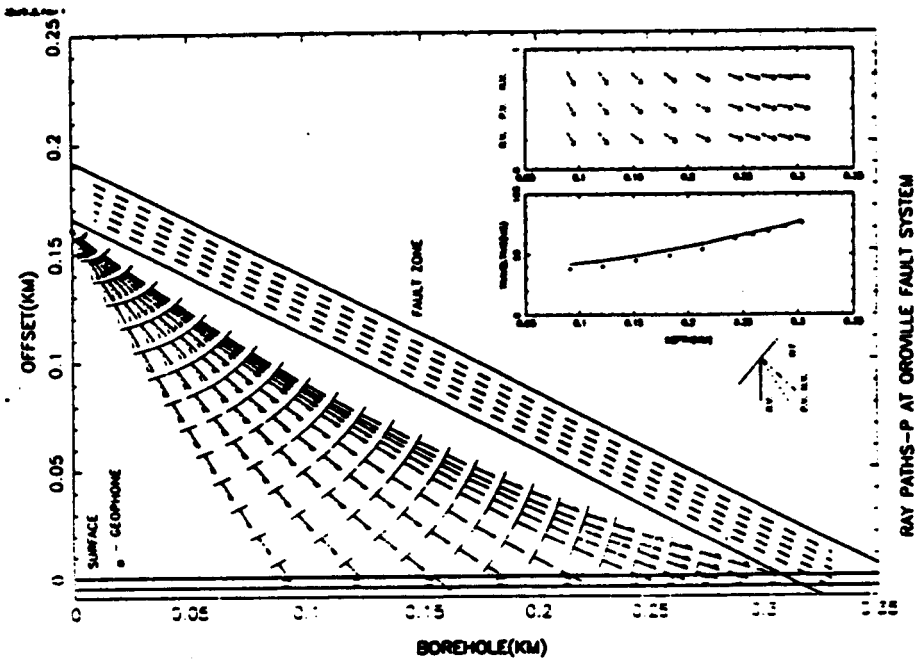
OFFSET(KM)
BOREHOLE(KM)
FAULT ZONE
SURFACE
• - GEOPHONE
RAY PATHS-P AT OROVILLE FAULT SYSTEM

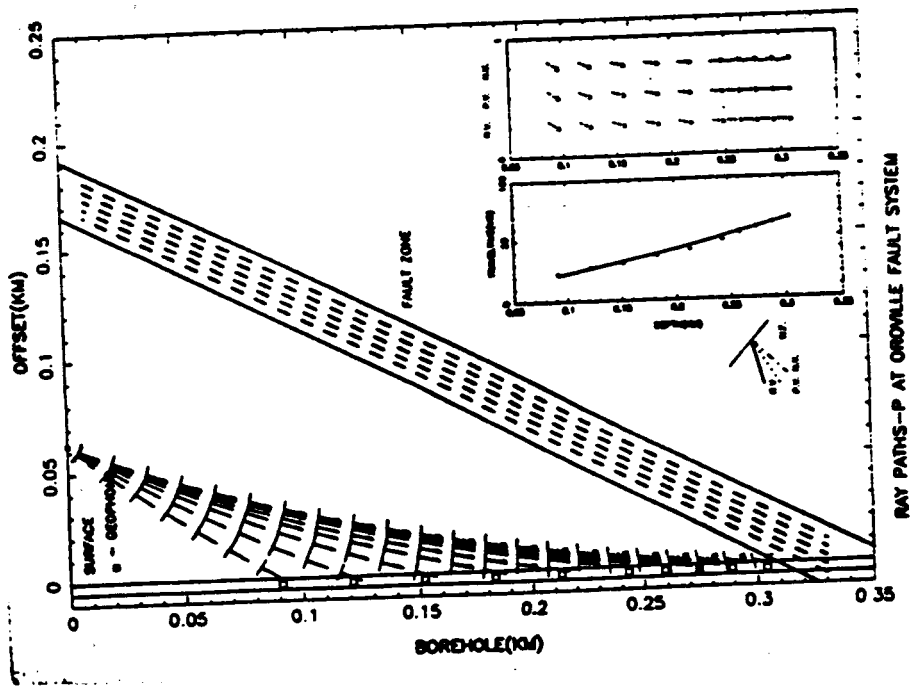
OFFSET(KM)
BOREHOLE(KM)
FAULT ZONE
SURFACE
• - GEOPHONE
RAY PATHS-P AT OROVILLE FAULT SYSTEM

Fig. 3

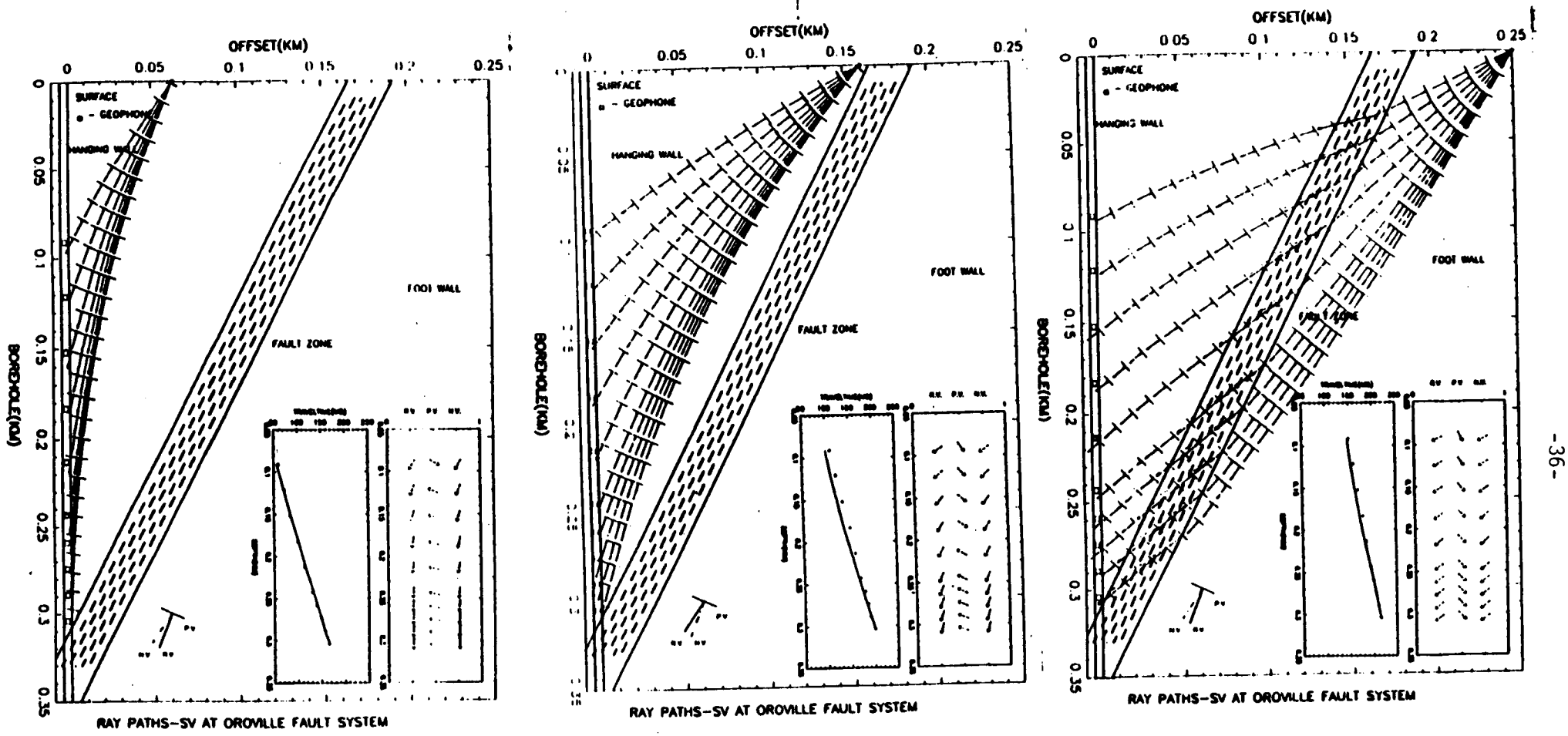
OFFSET(KM)
0
0.05
0.1
0.15
0.2
0.25
SURFACE
- GEOPHONE
HANGING WALL
FOOT WALL
FAULT ZONE
BOREHOLE(KM)
RAY PATHS-SV AT OROVILLE FAULT SYSTEM

Fig. 4

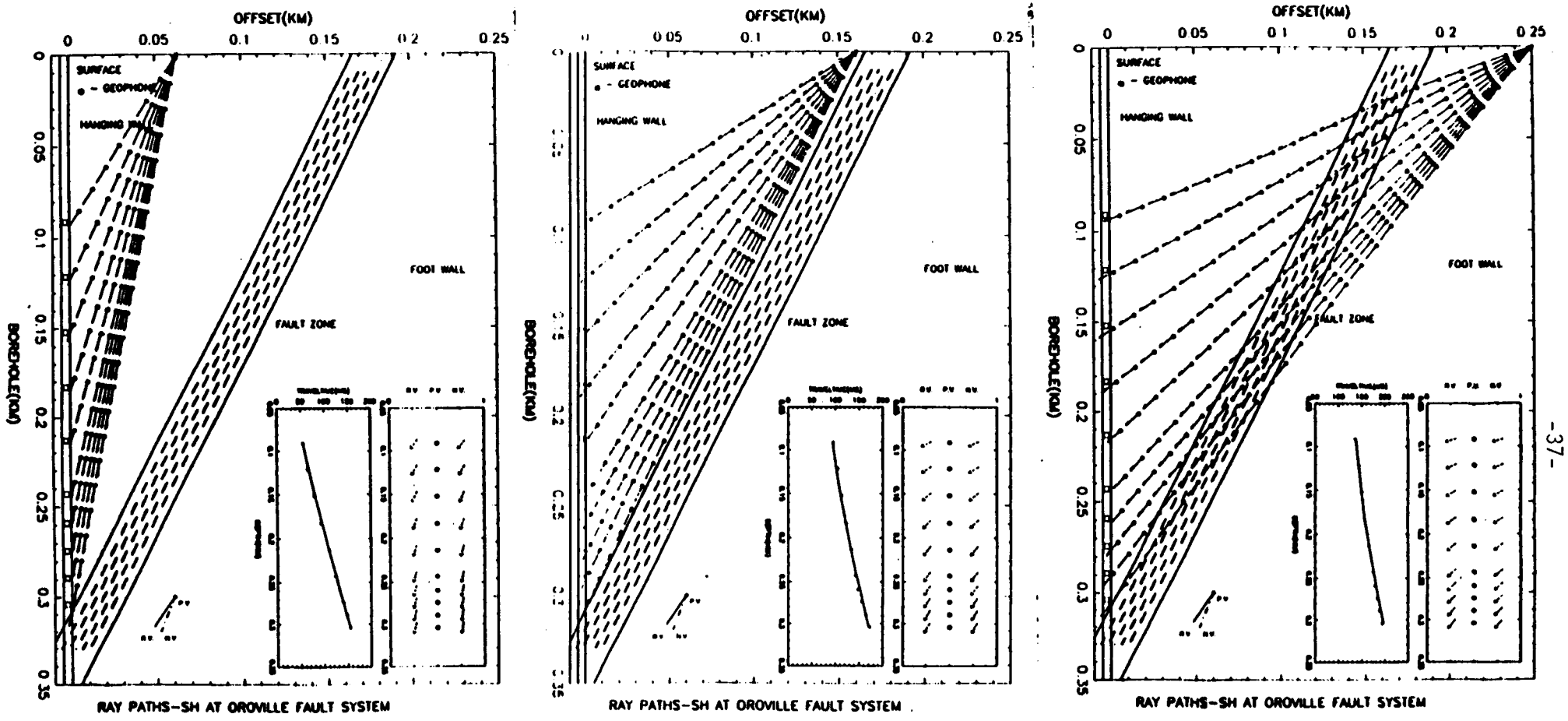
OFFSET(KM)
0
0.05
0.1
0.15
0.2
0.25
SURFACE
● - GEOPHONE
HANGING WALL
FOOT WALL
FAULT ZONE
BOREHOLE(KM)
RAY PATHS-SH AT OROVILLE FAULT SYSTEM

Fig. 5

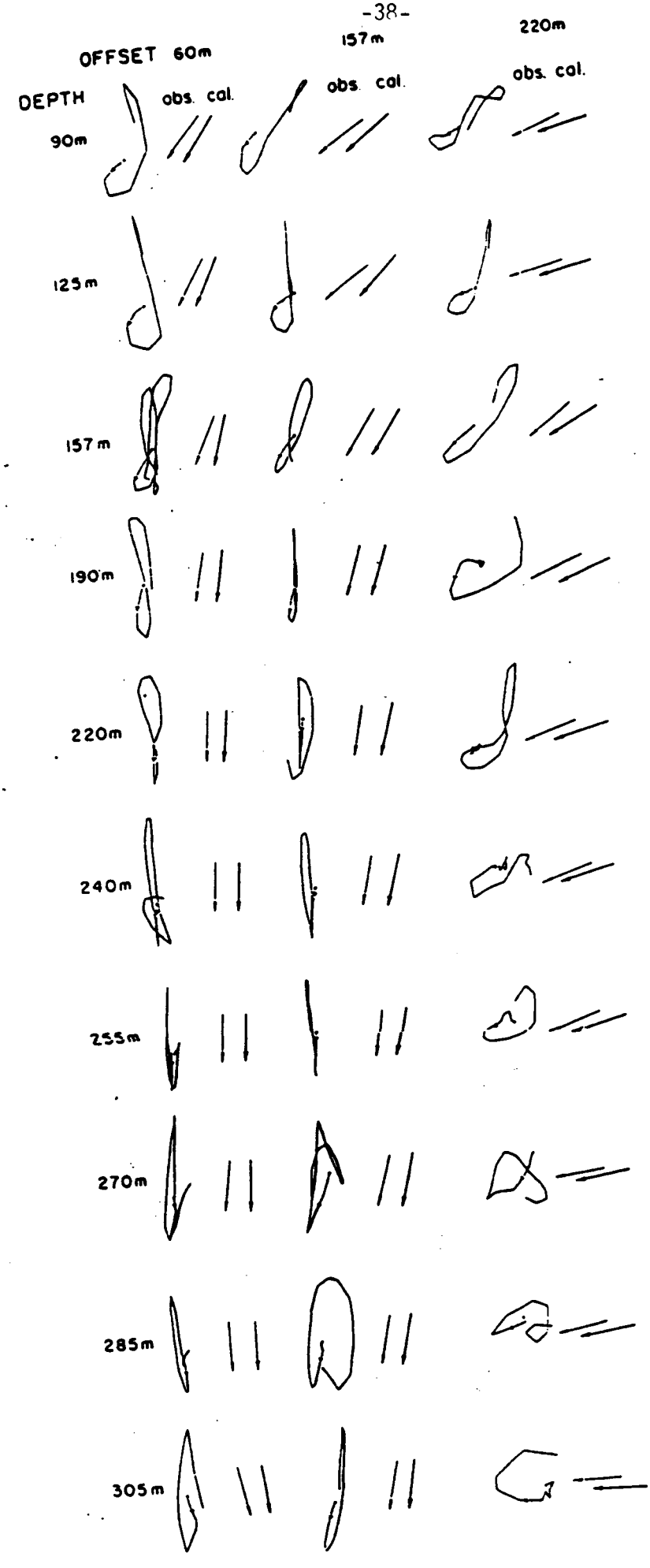
OFFSET 60m
157m
220m
DEPTH
obs. cal.
obs. cal.
obs. cal.
90m
125m
157m
190m
220m
240m
255m
270m
285m
305m

Fig. 6

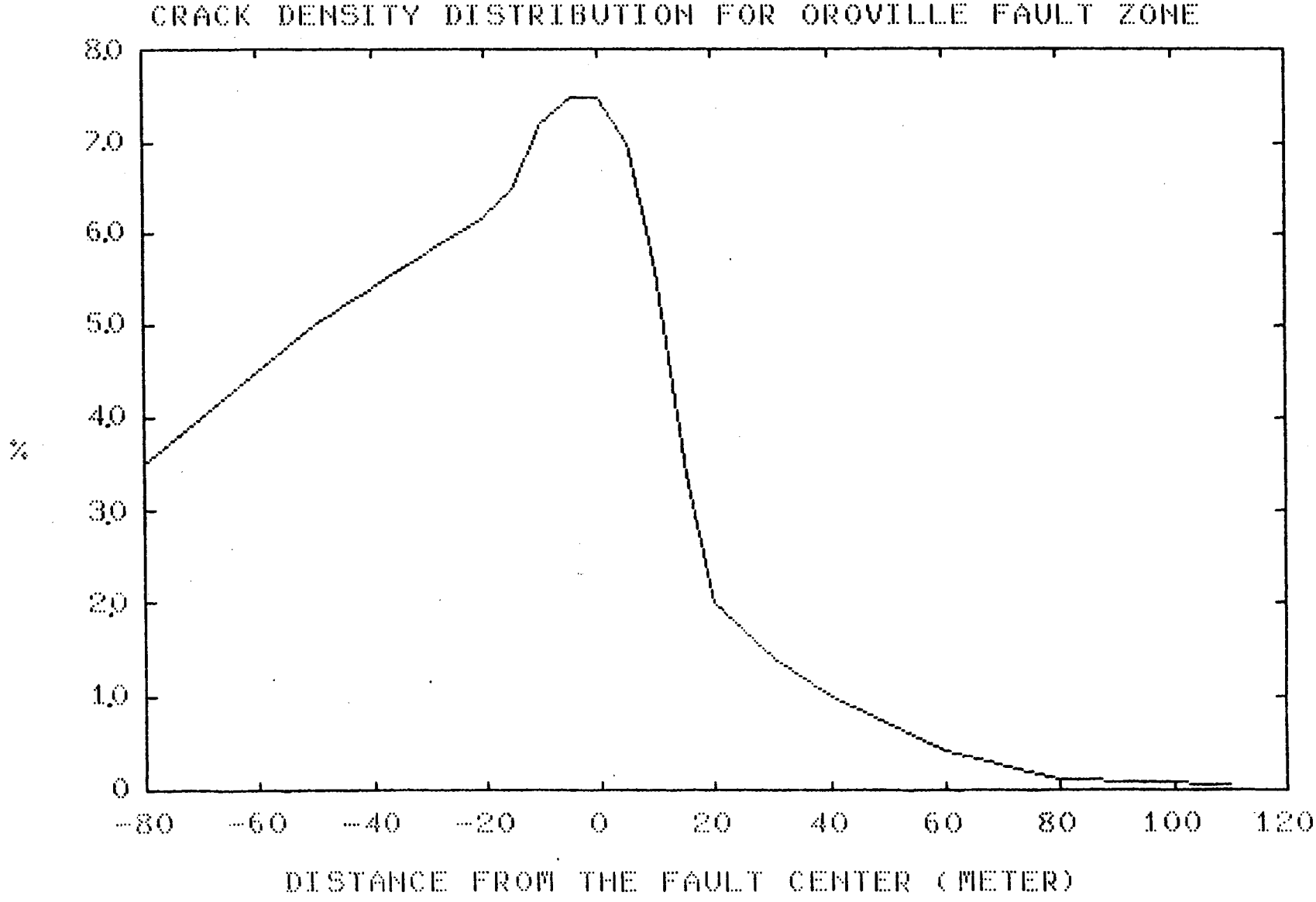
CRACK DENSITY DISTRIBUTION FOR OROVILLE FAULT ZONE
8.0
7.0
6.0
5.0
4.0
3.0
2.0
1.0
0
%
-80
-60
-40
-20
0
20
40
60
80
100
120
DISTANCE FROM THE FAULT CENTER (METER)

Fig. 7

(4) Development of a powerful new method for calculating seismic motions in media with irregular topography and interfaces by the superposition of Gaussian Beams.

Despite recent development in the theory of Gaussian Beams to solve some seismological problems, since its introduction into seismology by Cerveny et al. (1982), there is a certain lack of experience in determining to what extent the advantages and limitations of the theory can be of practical importance.

Most of the earlier applications were actually given within the context of introducing the theory, assuming simplified cases and calculating synthetic travel times and seismograms due to ideal incident seismic waves (Cerveny, 1983; Cerveny et al., 1983). Later on, only a few hard tests were performed for more complicated cases in 2-D (Nowack and Aki, 1983) and 3-D (Klimes and Cerveny, 1983) and on vertically heterogeneous media (Madariaga, 1983). Applications to study the crust-lower lithosphere using an efficient dynamic ray tracing has been performed by Muller (1983) and a hybrid method which combines both the Gaussian beam and the normal mode theories has been applied to calculate the waveform synthesis of surface waves in laterally heterogeneous earth (Yomogida and Aki, 1984). These works have contributed to estimate the capabilities of the Gaussian beam solution in dealing with problems that seismologists meet in real cases.

In this work we will try to contribute to this purpose by applying the theory to calculate the scattered waves in a homogeneous half-space with an irregular topography. An important feature of the gaussian beam solution, of practical value in this problem, is that it is regular at every point where the field is to be calculated, overcoming problems inherent to other methods, such as the breakdown of the ray theory at caustics and the instability of the source point discretization of the boundary integral method.

The general expression for an individual gaussian beam representing a SH-wave in a homogeneous medium is:

$$v_\delta(s,n,\omega) = G(s_0)\left(\frac{s_0 - iL_0^2}{s - iL_0^2}\right)^{1/2} e^{-i\omega[t-\tau(s,n)]} \exp\left(-\frac{n^2}{[L(s)]^2}\right) \qquad (1)$$

where:

s, n are the ray-centered coordinates, s_0 the ray coordinate of the beam's origin point, (Figure 1)

$G(S_0)$ is the initial amplitude,

$$L(s) = L_M\left[1 + \left(\frac{\lambda s}{\pi L_M^2}\right)^2\right]^{1/2}$$ is the width of the

beam, which varies along the ray path from an initial width L_M at s_0 for a given circular frequency ω. A more convenient parameter L_0 independent of frequency can be defined by

$$L_M = (2\beta/\omega)^{1/2} L_0,$$

$$\tau(s,n) = \frac{1}{\beta}[s + 1/2\ K(s)\ n^2],\quad K(s) = \frac{1}{s\left[1 + \left(\frac{\pi L_M^2}{\lambda s}\right)^2\right]}$$

The quantity K(s) can be interpreted as the curvature of the wave front as a function of distance s measured along the central ray.

$$\frac{K(s)\, n^2}{2\beta}$$

represents a time delay at a point off the central ray relative to the travel time at the central ray. The complex valued function

$$J^{1/2}(s) = \left(\frac{s - iL_0^2}{s_0 - iL_0^2} \right)^{1/2}$$

is calculated such that $-\pi \leq \arg(J(s)) \leq \pi$ for $s \geq s_0$, i. e., along the principal branch.

Since a single Gaussian beam has little, or perhaps no relevance in seismology, we are driven to represent our total wave field due to the incident and scattered waves as a superposition of many beams propagating at different directions. The incident wave can be a beam representation of a plane wave or a line source (Nowack and Aki, 1983). To represent the scattered waves we select P points along the topography and shoot Q beams from each point (Figure 2), at different take-off angles, covering a broad range of directions. The ray-centered coordinates are calculated in terms of the geographical coordinates and the take-off angles in a simple way, since the medium is homogeneous. The total field is then expressed by:

$$v(s,n) = G_0\, v_{0k} + \sum_{p=1}^{P} \sum_{q=1}^{Q} G_{pq}\, v_{pq}(s,n) \qquad (2)$$

where k is a parameter characterizing the source beams, with amplitudes Go, and G_{pq} are the complex amplitudes of the beam originated at p-th point in the direction q. The dependency on ω is understood. We calculate the coefficients G_{pq} by imposing the boundary conditions along the free surface in the least squares sense.

To do this, let us assume an error θ in the values of tractions at points i along the surface:

$$\left.\frac{\partial v}{\partial n}\right|_{z = J(x_i)} = \theta(x_i) \tag{3}$$

where J(x) is a function describing the topography. We minimize the squared errors integrated along the free surface,

$$\varepsilon = \int_J \left| \frac{\partial v}{\partial n} \right|^2_{z=J(x)} dx \tag{4}$$

with respect to each coefficient, according to:

$$\frac{\partial \varepsilon}{\partial G_{pq}} = 0 \tag{5}$$

Putting equation (2) into (5) yield the linear system of P x Q equations which is solved for G_{pq}.

$$\sum_{p,q} A_{ilpq}\, G_{pq} = b_{il}$$

where: (6)

$$A_{pqil} = \int \frac{\partial v_{il}^{*}}{\partial n} \frac{\partial v_{pq}}{\partial n}\, dx$$

$$b_{pq} = \int_{J} \frac{\partial v^{*}_{il}}{\partial n} \left(-G_{o} \frac{\partial v_{ok}}{\partial n}\right) dx$$

and $i = 1,---, P$, $l = 1,---, Q$ are dummy indices.

In equation 6, A_{ilpq} represents the constraint imposed over the traction due to the beam at $\underline{i}$ in the direction $\underline{l}$ by all the values of the tractions due to the beam at $\underline{p}$ in the direction $\underline{q}$ along the surface. b_{il} represents the constraints imposed by the source.

As an example for illustrating our method, we consider the problem of vertically incident plane SH waves upon a canyon of sinusoidal shape (Figure 3a). Our results are compared with those obtained by Bouchon for a similar case using the Aki-Larner method (1973). Following Bouchon, we study incident waves having wavelength $\lambda = 5h$, where h is chosen as a fraction of the half width w. A reasonable agreement with Bouchon's result is obtained for, h = 0.8, 0.53, 0.4 times w, which correspond to rather steep topography. Interestingly, unlike the Aki-Larner method, our method gives more stable result for rough topography than smooth one, because of the matrix singularity for the case of flat topography. Since the Aki-Larner method is most stable for the flat case, the two approaches may compensate each other.

Further testing of our method was made using the case of semi-circular canyon. Results are compared with the closed form exact solution for the total field obtained by Trifunac (1973). The amplitude of the displacement at

the surface is shown against the normalized frequency

$$\eta = \frac{\omega W}{\pi \beta} = \frac{2W}{\lambda}$$, for η = 0.75, 1.0, 1.25, 1.75 and 2.0 (Figure 4).

From these examples we immediately notice that, although there is a good local agreement of the gaussian beam solution within the interval -W, W with both Aki-Larner and Trifunac solution, the solution outside the interval is in general poorly matched. We found that the scattered wave field is highly sensitive to the choice of parameter L_0 which determines the initial beam width.

In figure 5 the residual stress at the surface is calculated for different values of L_0. The best match of the boundary conditions occurs for L_0 = 1.3 km$^{-1/2}$ and large residuals occur for a departure of as little as 0.4 from L_0. We notice also that the optional values of L_0 may depend on the frequency. Every scattered beam is characterized by a unique L_0, at any point along the surface. Obviously, this decreases the resolution at points of strong diffraction (at the border of the circular cannyon for example) whenever we chose a wide L_0 to satisfy the boundary conditions at the flat surface.

The optimal choice of L_0 in terms of other parameters of a given scattering problems is still to be investigated. The fact that the solution is poor outside the valley is probably due to two reasons: Firstly, we consider the beam source points only in and near the valley and truncate the outside contributions. Secondly, there is no representation of inhomogeneous waves in our gaussian beam synthesis.

Regarding the stability of the least squares approximation in our method as mentioned earlier it is more stable when the slope of the irregularity is stronger or when frequencies are higher. This can be seen from the expression

for the matrix A_{ijpq}; products of derivatives with respect to the normal are integrated along the topography. If the irregularity is smooth, neighbored beams are not very distinct from each other and make A an ill-conditioned operator. This problem can be eliminated if we determine the beam amplitude in the wave number domain as was done in the Aki-Larner method. We are very much excited by this initial success, because the Gaussian beam synthesis method described above can be extended to the heterogeneous medium with irregular topography and discontinuities in a straight-forward manner.

FIGURE CAPTIONS

Figure 1. Gaussian "bell-shaped" solution of the elastodynamic wave equation concentrated close to the ray Ω. The unit vectors $\underline{t}$ and $\underline{n}$ are tangential and normal to the ray at the observation point P respectively. The distance s is measured along the ray from the origin point S_0.

Figure 2. Source point discretization of the topography. From a selected point p, Q beams are shot at different directions to represent the scattered waves. α is the slope of the irregularity at ρ. An incident plane wave is represented by a superpositon of Gaussian beams depending on the parameter k.

Figure 3. Comparison of the normalized displacement amplitudes due to a vertically incident SH plane wave upon a sinusoidal canyon calculated by using (a) Gaussian beams and (b) Aki-Larner techniques.

Figure 4. Comparison of the displacement amplitudes due to vertically incident SH plane wave upon a circular canyon, calculated by using (a), (b) Gaussian beams and (c) the analytic solution obtained by Trifunac. η is a normalized frequency defined by $\eta = \frac{\omega W}{\pi\beta} = \frac{2W}{\lambda}$. No Gaussian beam solution is shown for η=0.25 and η=0.50.

Figure 5. Residuals of the shear stress calculated at the surface by using Gaussian beams for the case shown in Figure 4 (c). The effect of Lo, the initial beam width parameter, is emphasized.

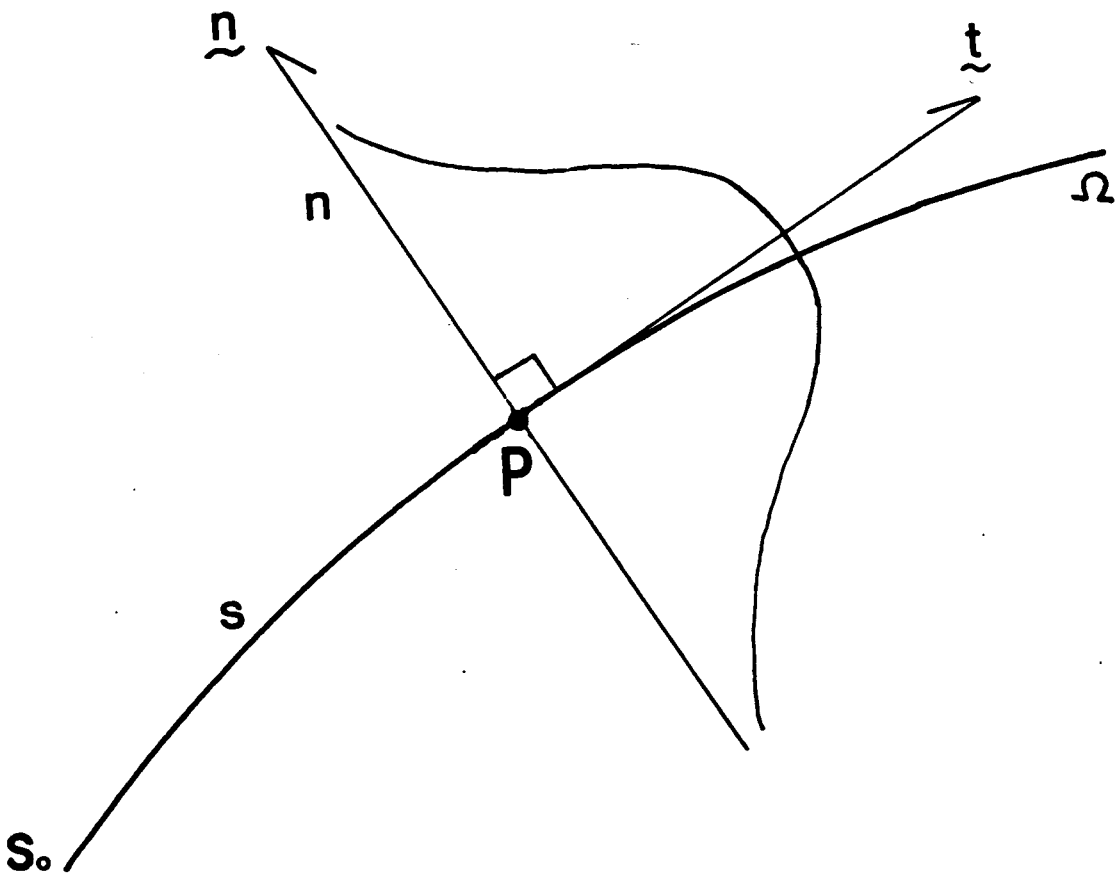

FIGURE 1

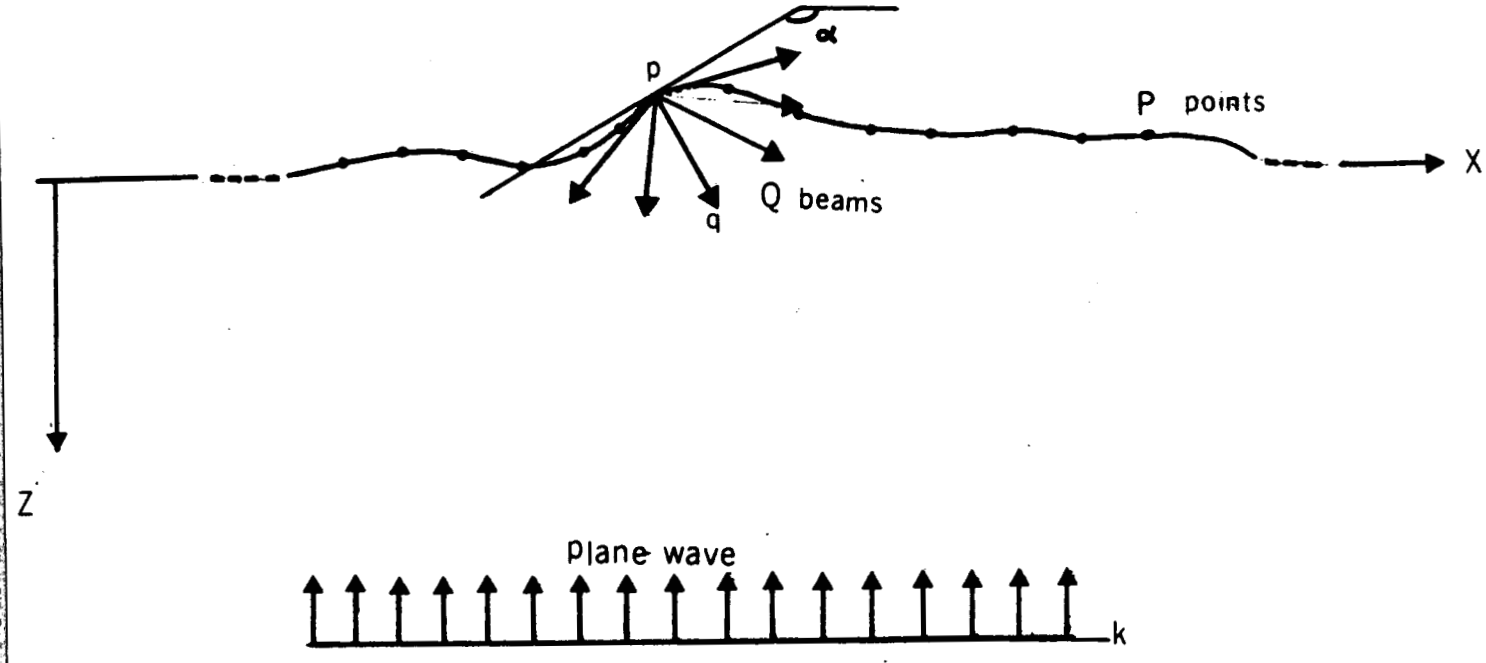

FIGURE 2

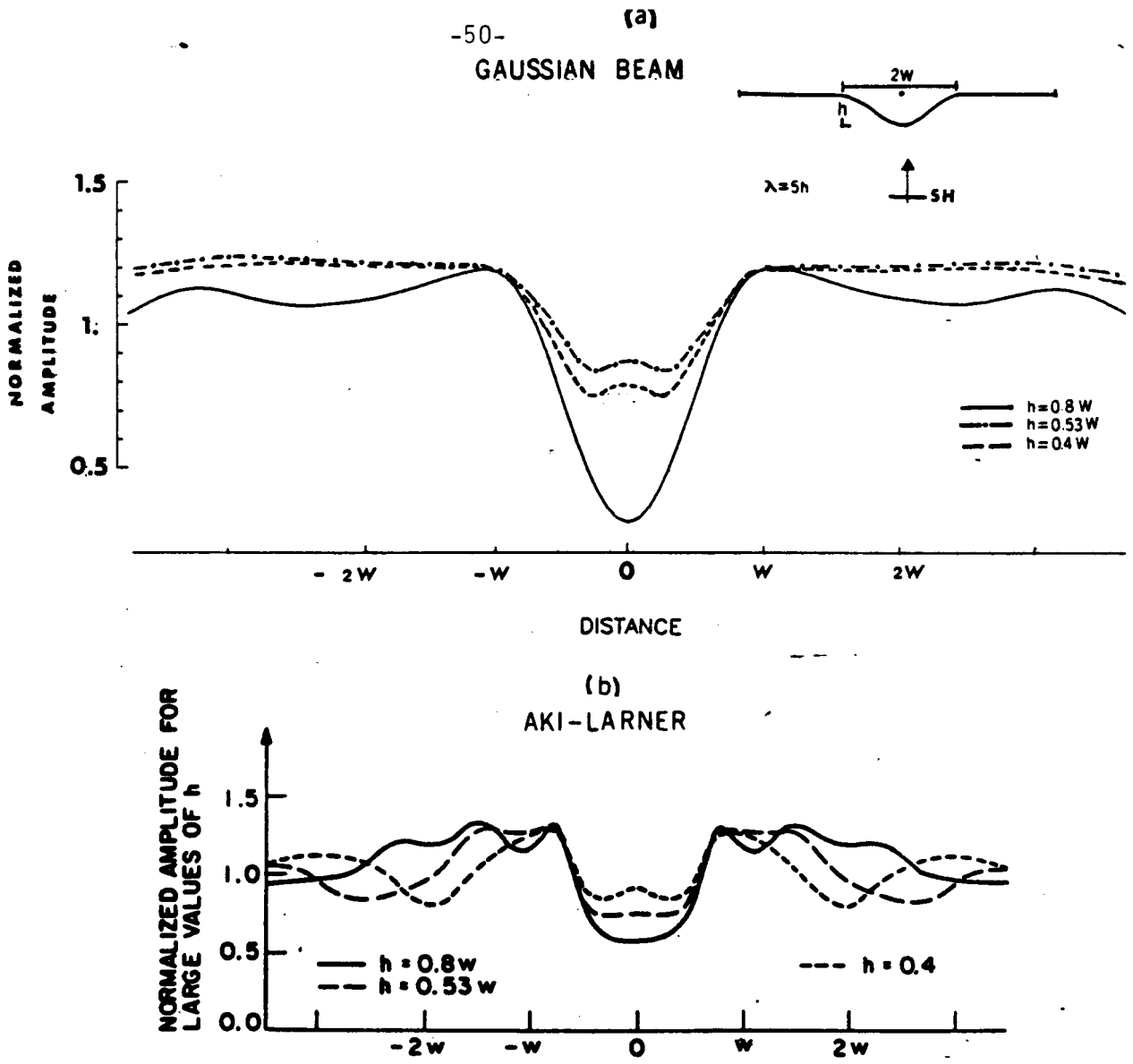
(a)
GAUSSIAN BEAM
2W
h
λ=5h
SH
1.5
1.
0.5
NORMALIZED AMPLITUDE
h=0.8 W
h=0.53W
h=0.4W
- 2W
-W
0
W
2W
DISTANCE
(b)
AKI-LARNER
NORMALIZED AMPLITUDE FOR LARGE VALUES OF h
1.5
1.0
0.5
0.0
h = 0.8w
h = 0.53 w
--- h = 0.4
-2w
-w
0
w
2w

FIGURE 3

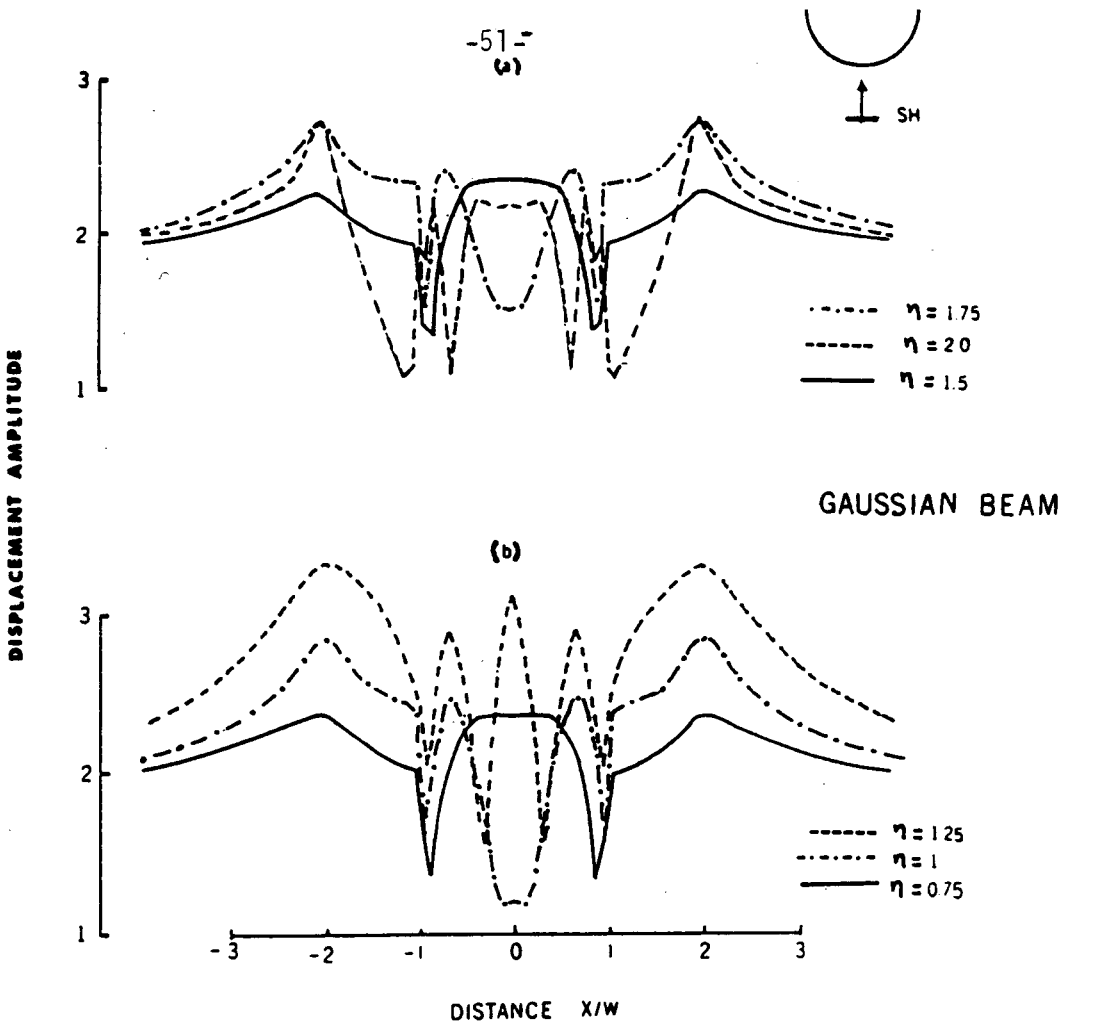

GAUSSIAN BEAM

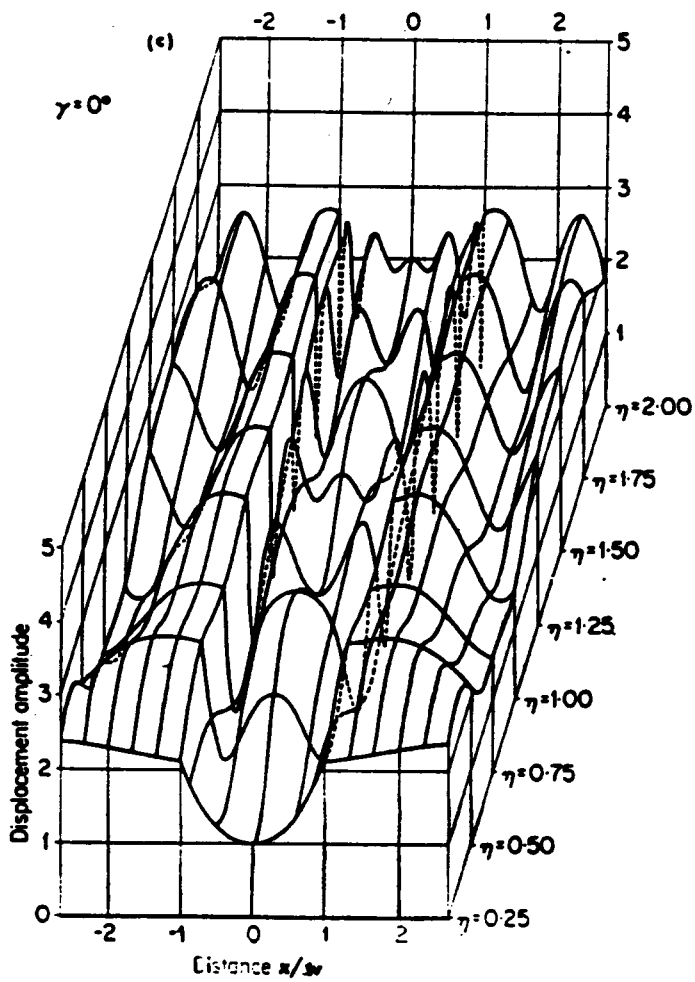

TRIFUNAC

FIGURE 4

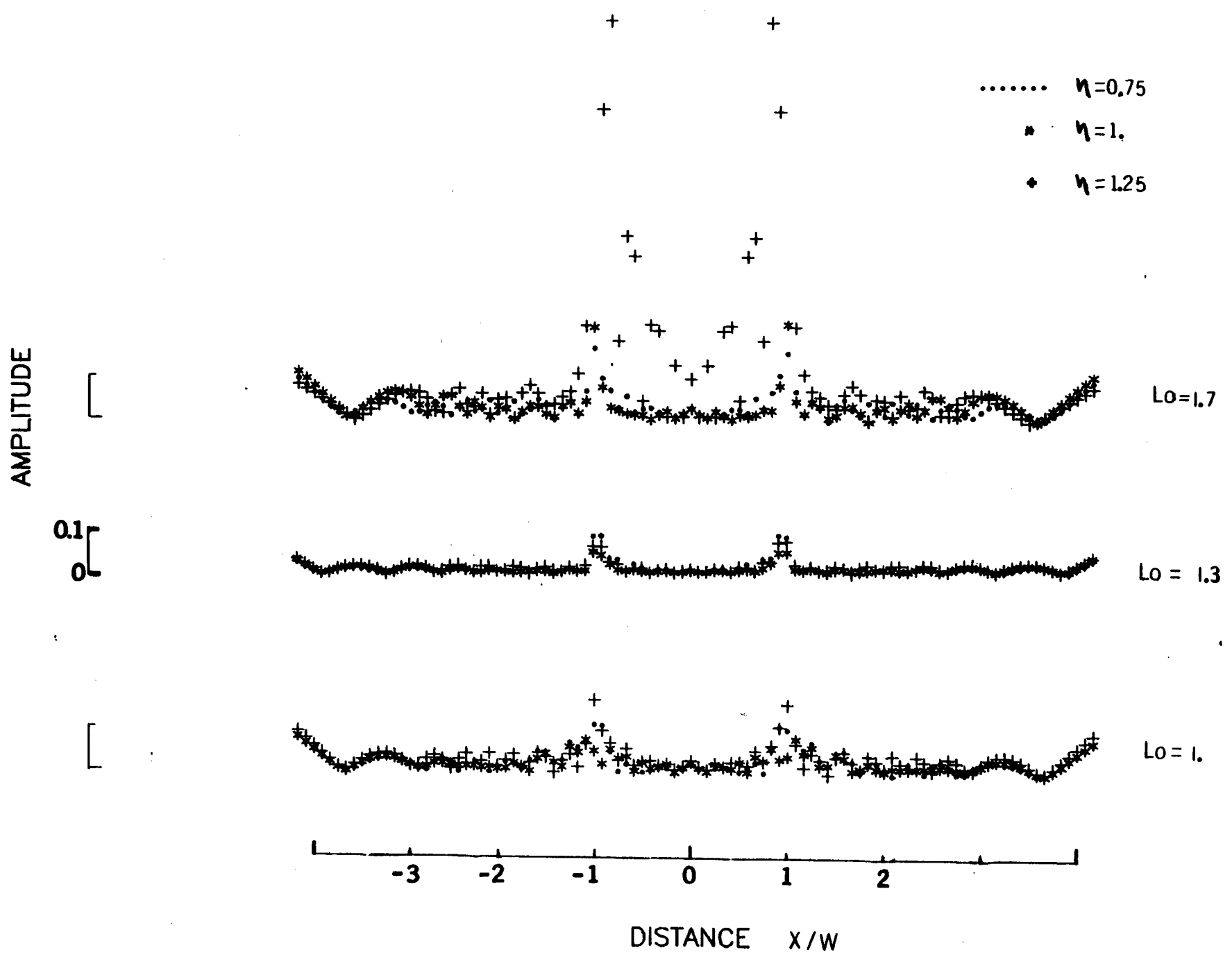

FIGURE 5

REFERENCES

Aki, K., B. Chouet, M. Fehler, G. Zandt, R. Koyanagi, J. Colp, and R. G. Hay, Seismic properties of a shallow magma reservoir in Kilauea Iki by active and passive experiments, J. Geophys. Res., 83, 2273-2282, 1978.

Aki, K., M. Fehler and S. Das, Source mechanism of volcanic tremors: Fluid driven crack models and their application to the 1963 Kilauea eruption, J. Volcan. Geotherm. Res., 2, 259-287, 1977.

Aki, K., and R. Koyanagi, Deep volcanic tremor and magma ascent mechanism under Kilauea, Hawaii, J. Geophys. Res., 86, 7095-7109, 1981.

Aki, K. and K. L. Larner, Surface motion of a layered medium having an irregular interface due to incident plane SH waves, J. Geophys. Res., 75, 933-954, 1970.

Aki, K. and P. G. Richards, Quantitative Seismology: Theory and Methods, Vol. 1, W. H. Freeman, 1980.

Babich, V. M. and M. M. Popov, Propagation of concentration sound beams in a three-dimensional inhomogeneous medium, Sov. Phys. Acoust., 27, 459-462, 1981.

Bame, D. A. and M. C. Fehler, Observational long-period earthquakes accompanying hydraulic fracturing, Geophys. Res. Lett., 13, 144-152, 1986.

Cerveny, V. and I. Psencik, Rays and travel times of seismic body waves in inhomogeneous slightly anisotropic media, Geophys. J. R. astr. 76, 157-163, 1972.

Cerveny, V., Expansion of a plane wave into Gaussian beams, Stud. Geophys. Geod., 26, 120-131, 1982.

Cerveny, V. and I. Psencik, Gaussian beams and paraxial ray approximations in three-dimensional elastic inhomogeneous media, J. Geophys., 53, 1-15, 1983a.

Cerveny, V. and I. Psencik, Gaussian beams in two-dimensional elastic inhomogeneous media, Geophys. J. R. astro. Soc., 72, 417-433, 1983b.

Chouet, B., Dynamics of a fluid driven crack in three dimensions by finite difference method, J. Geophys. Res., in press, 1986.

Chouet, B., Excitation of a buried magmatic pipe: a seismic source model for volcanic tremor, J. Geophys. Res., 90, 1881-1893, 1985.

Chouet, B., Free surface displacements in the near field of a tensile crack expanding in three dimensions, J. Geophys. Res., 87, 3868-3872, 1982.

Cormier, V., An application of the propagator matrix of dynamic ray tracing: the focusing and defocusing of body waves by three-dimensional velocity structure in the source region, Geophys. J. R. astr. Soc., 87, 1159-1180, 1986.

Eichelberger, J. C. and W. Hildreth, Research drilling at Katmai, EOS, 67, 778-780, 1986.

Eichelberger, J. C., P. C. Lysne, C. D. Miller and L. W. Yonker, Research drilling at Inyo domes, California: 1984 results, EOS, 66, 186-187, 1985.

Fehler, M. and B. Chouet, Operation of a digital seismic network on Mount St. Helens volcano and observations of long period seismic events that originate under the volcano, Geophys. Res. Letters, 9, 1017-1020, 1982.

Fehler, M. C., Observation of volcanic tremor at Mt. St. Helens volcano, J. Geophys. Res., 88, 3476-3484, 1983.

Hanyga, A., Gaussian beams in anisotropic elastic media, Geophys. J. R. astr. Soc., 85, 473-503, 1986.

Hudson, J. A., Wave speeds and attenuation of elastic waves in material containing cracks, Geophys. J. R. astr. Soc., 64, 133-150, 1980.

Nakamura, K., Volcanoes as possible indicators of tectonic stress orientation - principle and proposal, J. Volcan. Geoth. Res., 2, 1-16, 1977.

Nowack, R. and K. Aki, The two-dimensional Gaussian beam synthesis method: Testing and application, J. Geophys. Res., 89, 7747-7819, 1984.

O'Connell, R. S. and B. Budiansky, Seismic velocities in dry and saturated cracked solid, J. Geophys. Res., 79, 5412-5426, 1974.

Popov, M. M., A new method of computation of wave fields using Gaussian beams, Wave Motion, 4, 85-97, 1982.

Trifunac, M. D., Scattering of plane SH waves by a semi-cylindrical canyon, Int. J. Earthquake Eng. Struct. Dyn., 1, 267-281, 1973.

Yomogida, K. and K. Aki, Waveform synthesis of surface waves in a laterally heterogeneous earth by the Gaussian beam method, J. Geophys. Res., 90, 7665-7688, 1985.